



LAWRENCE
LIVERMORE
NATIONAL
LABORATORY

LLNL-JRNL-839286

Critical Exploration of Liquid Metal Plasma Facing Components in a Fusion Nuclear Science Facility

C. E. Kessel, D. Andruczyk, J. P. Blanchard, T. Bohm, A. Davis, K. Hollis, P. W. Humrickhouse, M. Hvasta, M. Jaworski, J. Jun, Y. Katoh, A. Khokak, J. Klein, E. Kolemen, G. Larsen, R. Majeski, B. J. Merrill, N. B. Morley, G. H. Neilson, B. Pint, M. E. Rensink, T. D. Rognlien, A. F. Rowcliffe, S. Smolentsev, M. S. Tillack, L. M. Waganer, G. M. Wallace, P. Wilson, S. J. Yoon

August 29, 2022

Fusion Science and Technology

Disclaimer

This document was prepared as an account of work sponsored by an agency of the United States government. Neither the United States government nor Lawrence Livermore National Security, LLC, nor any of their employees makes any warranty, expressed or implied, or assumes any legal liability or responsibility for the accuracy, completeness, or usefulness of any information, apparatus, product, or process disclosed, or represents that its use would not infringe privately owned rights. Reference herein to any specific commercial product, process, or service by trade name, trademark, manufacturer, or otherwise does not necessarily constitute or imply its endorsement, recommendation, or favoring by the United States government or Lawrence Livermore National Security, LLC. The views and opinions of authors expressed herein do not necessarily state or reflect those of the United States government or Lawrence Livermore National Security, LLC, and shall not be used for advertising or product endorsement purposes.

Critical Exploration of Liquid Metal Plasma Facing Components in a Fusion Nuclear Science Facility

C. E. Kessel^{a,f*}, D. Andruszyk^b, J. P. Blanchard^c, T. Bohm^c, A. Davis^c, K. Hollis^d, P. W. Humrickhouse^e, M. Hvasta^a, M. Jaworska^a, J. Jun^f, Y. Katoh^f, A. Khodak^a, J. Klein^g, E. Kolemen^a, G. Larsen^g, R. Majeski^a, B. J. Merrill^e, N. B. Morley^h, G. H. Neilson^a, B. Pint^f, M. E. Rensinkⁱ, T. D. Rognlienⁱ, A. F. Rowcliffe^f, S. Smolentsev^h, M. S. Tillack^j, L. M. Waganer^k, G. M. Wallace^l, P. Wilson^c, S-J. Yoon^e

^a*Princeton Plasma Physics Laboratory, Princeton, NJ, USA*

^b*University of Illinois, Campaign-Urbana, IL, USA*

^c*University of Wisconsin, Madison, Wisconsin, USA*

^d*Los Alamos National Laboratory, Los Alamos, New Mexico, USA*

^e*Idaho National Laboratory, Idaho Falls, Idaho, USA*

^f*Oak Ridge National Laboratory, Oak Ridge, TN, USA*

^g*Savannah River National Laboratory, Jackson, South Carolina, USA*

^h*University of California, Los Angeles, California, USA*

ⁱ*Lawrence Livermore National Laboratory, Livermore, California, USA*

^j*University of California, San Diego, California, USA*

^k*Consultant, 10 Worcester Ct., O'Fallon, Missouri, USA*

^l*Massachusetts Institute of Technology, Cambridge, Massachusetts, USA*

Abstract

1.0 Introduction

The development of long lifetime plasma facing components (PFCs) provides a significant barrier to the success of fusion energy. These materials will see both the high-energy neutrons from the plasma and high plasma and neutral fluxes to their surfaces. The associated heat and particle fluxes, and volumetric heating will give rise to material evolution and high temperatures with significant gradients. The nuclear damage and transmutation production is a maximum at the plasma-facing surface. Plasma exposure will erode and re-constitute the surface materials (through re-deposition and migration). The application of a liquid layer for the plasma-facing component has the potential to alleviate some of the extreme conditions a solid PFC would need to endure. This paper is reporting the examination of liquid metals (LM) PFCs in the Fusion Nuclear Science Facility [1], and accompanying papers will provide detailed assessments in specific areas [2-8]. The study is roughly separated into four areas 1) liquid metal characteristics, 2) solid substrate characteristics and interactions, 3) integration issues associated with these LM PFCs, and 4) specific first wall and divertor concepts. For this activity the liquid metal PFC is added on top of an otherwise conventional breeding blanket, and/or in the divertor, and therefore is relatively thin, ≤ 2.5 cm. The actual thickness of the liquid metal layer will be determined by a number of trade-offs in the design of the concept (e.g. MHD, heat transfer, exposure distance, capillary). The liquid metal will require a solid substrate. The LM PFC will introduce another fluid system into the fusion core, in addition to the main coolant He and breeder PbLi, the Dual Coolant Lead Lithium (DCLL) blanket used in the FNSF is assumed.

Asking the question of why consider a liquid layer on the plasma facing surfaces the primary reasoning includes

1. eliminate plasma degradation of a solid PFC (erosion, re-constitution) as a lifetime limit
2. removal of the surface heat load that would be seen with a solid PFC
3. reduce the nuclear damage and transmutation that would be seen by a solid PFC
4. reduce the largest gradients (damage, temperature, stress) that would be seen in a solid PFC

In general, it is understood that a liquid metal layer would accomplish all of these and is the main motivation to examine their potential. Different concepts, such as flowing or capillary, would accomplish this to differing degrees primarily due to differing thickness of the liquid layer, and what the liquid material is. This study is intended to identify what critical R&D is needed to understand the liquid metal behavior in the fusion environment, how specific concepts apply in a fusion nuclear facility (FNSF), and steps to confirm the credibility of liquid metal as a PFC in a reasonable timeframe. This can be contrasted with previous activities targeting large neutron and surface heat fluxes as their goal [9,10]. Numerous reviews and progress reports have been made recently in the area of liquid metal PFCs [11-13], although this is not exhaustive, that span experimental facilities, concepts, and facilities where liquid metals or PFC surface coatings are applied.

The primary goal of research in the LM PFC area is to develop a technical basis for a practical system that can be applied to a fusion device. The prospect of using liquid metals as plasma facing components requires a series of R&D activities that can establish the viability of this approach and to do it in an expedient way. Although one can answer “yes” to the potential benefits of a liquid metal layer on solid substrates in a fusion device, posed in the Introduction, the viability of a workable LM system remains unknown. This unknown presents a significant barrier to adopting LMs as the solution to the challenging PFC problem in fusion. However, establishing a focused program on resolving issues and uncertainties with an eye toward integrated and prototypical systems is the motivation of this report and study into LM PFCs. In this context the LM PFC issues are opportunities, and they remain issues only until we resolve them or circumvent them.

2.0 Liquid metal properties

Liquid metals have several properties that require attention when applying them to plasma facing surfaces. The low melting point metals in the periodic chart can be scanned for their vapor pressure (evaporation rate) and nuclear responses, as well as a number of other properties. Most of these metals can be rejected based on the evaporation rate over temperature ranges of interest (~ 350 - 800 $^{\circ}\text{C}$), leaving Sn, Sn-Li, Ga, Ga-Li, In, In-Li, and Pb-Li. Li is also retained for operation at the lower temperature range or in a high evaporation regime, and Pb-Li is retained for comparison due to its high breeding potential and blanket application. The evaporation rates are shown in Fig. 1 for the candidates, although In-Li data is not available. The evaporation rates for Pb-Li and Sn-Li are determined using activity coefficients from [14]. Phase diagrams exist for Sn-Li [15], Pb-Li [16], and In-Li [17], all showing similar trends with low melting temperatures at the lower Li concentration range, and higher melting temperatures and

multiple inter-metallics at the higher Li concentration range. The phase diagram for Ga-Li [18] shows different behavior, with a rapidly rising melting temperature with increasing Li content, at lower Li content range (e.g. 500 °C at 20 at % Li), and a falling melting temperature with rising Li content, at the higher Li content range (e.g. 260 °C at 90 at % Li). Appropriate levels of Li in Sn-Li range from a few to 25% before the melting temperature rises rapidly, while in In-Li the Li level might range from a few to 15%. Pb-Li has a eutectic (minimum melting temperature over constituency range, except 100% Li) concentration around 15.7% Li and 84.3% Pb (forming a V liquidus line in the phase diagram), which restricts practical operation to avoid solidification and intermetallic formation due to a rapidly rising melting temperature on both sides of the eutectic composition. From the application point of view, any liquid metal must be operated well above its melting point ($T - T_{melt} > 50-100$ °C) since it must travel through an entire loop including the plasma chamber, tritium extraction, heat exchanger, and clean-up, while avoiding any solid precipitation (except possibly in the clean-up system).

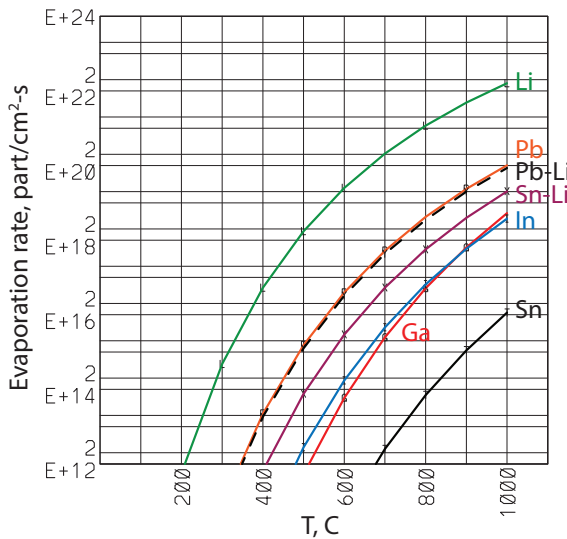


Figure 1. Evaporation rates for some liquid metal PFC candidates.

The operating temperature of a liquid metal in the plasma chamber, and subsequently in the overall loop in a fusion facility, is dictated by its evaporation rate (and other losses), intrinsic impurities in the liquid metal, impurities introduced into the liquid metal by corrosion, the heat load it receives and speed that it flows through the plasma chamber, and subsequent materials it interfaces outside the fusion core. This can be complicated by the introduction of large fluxes of hydrogen to the liquid metal while in the plasma chamber, possibly affecting its constituency and properties. The requirements of these external apparatus (e.g. tritium extraction) may provide additional constraints. For example, the technique for tritium extraction from a LM may be compromised by other impurities in the LM, requiring that they be removed in advance. The attractiveness of a liquid metal PFC for thermal energy conversion is determined by the maximum achievable temperature.

Ga and In are elements that are only recovered from the mining and purification of other materials, Al, Zn and Cu for example, and so are not mined directly since they are so dilute in the earth's crust. The by-product recovery of these elements has been sufficient

for industrial applications, however, requiring the recovery of a ton or more for each fusion power plant would require ramping up the mining of other metals. In addition, Ga has very aggressive corrosion of steels, including ferritic steels like reduced activation ferritic martensitic (RAFM) fusion steel. For these reasons the use of Ga and In, or their alloys, will no longer be considered, reducing the list of considered LMs to Li, Sn, Sn-Li, and Pb-Li.

2.1 Loss rate from liquid metal surfaces

The loss rate of a liquid metal in the plasma chamber plays a central role in its viability and operating temperature range. The physical sputter [19-21], ad-atom [22-26], and evaporation combination model is taken as the basis for determining this loss flux and can be given for Li by (for example),

$$\begin{aligned}\phi_{\text{loss}}^{\text{Li}} = & f_{\text{neut}} [\sum_j \phi_D(E_j) Y_{D,\text{Li}}(E_j) + \sum_j \phi_T(E_j) Y_{T,\text{Li}}(E_j) + \sum_j \phi_{\text{He}}(E_j) Y_{\text{He},\text{Li}}(E_j) \\ & + \sum_j \phi_{\text{Li}}(E_j) Y_{\text{Li},\text{Li}}(E_j) + \sum_j \phi_Z(E_j) Y_{Z,\text{Li}}(E_j)] \\ & + f_{\text{neut}}^{\text{ad}} \{\sum_j \phi_D(E_j) Y_{D,\text{Li}}^{\text{ad}}(E_j) + \sum_j \phi_T(E_j) Y_{T,\text{Li}}^{\text{ad}}(E_j)\} / (1 + A \exp(E_{\text{eff}}/kT)) \\ & + \phi_{\text{evap}}^{\text{Li}}(T)\end{aligned}$$

where $\phi_{D,T,\text{He},Z,\text{Li}}$ is particle flux on to the liquid metal (particles/m²/s), Y is the yield in atoms/ion or atoms/atom, f_{neut} and $f_{\text{neut}}^{\text{ad}}$ are the fraction of loss particles that are neutral (since charged particles are most likely returned to the surface within the sheath), Y^{ad} is the ad-atom yield (atoms/ion), A and E_{eff} are parameters for the ad-atom process, and $\phi_{\text{evap}}(T)$ is the normal thermal evaporation flux, given by $CP_{\text{vap}}(T)/(mT)^{1/2}$. The physical sputtering terms include D and T hydrogen ion, He ion, Li ion and other impurity (Z) ion bombardment, although the ad-atom loss is only shown for the hydrogen species bombardment. The summations are over the incident particle energies (energy groups). The ad-atom process involves a particle flux that excites near-surface atoms to reside on top of the surface where they undergo thermal evaporation. This is dependent on the flux (which provides the production of ad-atoms) and the impinging particle's energy (lower is more likely to produce ad-atoms due to shallow energy deposition). Both the fluxes to the surface and the yields are energy dependent. In general, ions hitting the surface would be perpendicular due to the sheath, while neutral particles can impinge from any angle. The emitted particles would also have some initial angular distribution. These angular dependences are suppressed in the loss equation shown above for clarity. This loss formulation is illustrated in Fig. 2, for Li, one of the few materials where the ad-atom parameters have been estimated [24, 25]. Here we use $A = 1.e-7$, $E_{\text{eff}} = 0.9$ eV, $Y_{D,\text{Li}} = 0.1$, $Y_{T,\text{Li}} = 0.1$, $Y_{\text{He},\text{Li}} = 0.16$, $Y_{\text{Li},\text{Li}} = 0.3$, $Y_{Z,\text{Li}} = 0$, $f_{\text{neut}} = 0.35$, $f_{\text{neut}}^{\text{ad}} = 1.0$, $Y_{\text{ad}}/Y_{\text{ps}} = 50$ (ratio of ad-atom yield to physical sputtering yield), $\phi_D = \phi_T = 0.5 \times 10^{20} / \text{m}^2\text{-s}$, $\phi_{\text{He},\text{Li}} = 0$, $\phi_{\text{Li}} = 0.65 \times 10^{20} / \text{m}^2\text{-s}$. The physical sputtering provides a constant loss term, and the evaporation rate grows continuously with temperature, while the ad-atom loss rises earlier than the evaporation and can lead to a higher loss rate at lower temperatures. The hydrogen fluxes used in this example were determined by 2D scrape-off layer plasma simulations for the FNSF [27], but may not be self-consistent with a Li plasma facing material. In general, most physical sputter yields are available for liquid Sn [20], Li [19], and Sn-Li [21], although the lower energy range (< 200eV) lacks data, and TRIM analysis has been used to fill in this region. Evaporation data is widely available. The

ad-atom physical parameters are motivated and simulated in [24, 25], but are still generally fits to the data, and are barely available experimentally. Fig. 2 illustrates the importance of characterizing the ad-atom loss channel, since at a given allowable flux of particles lost from the LM surface, there is a maximum temperature of operation. From previous results with 2D scrape-off-layer simulations for lithium [28], it was determined that a loss flux of 2×10^{20} Li particles/m²-s could be tolerated before diluting the core plasma too heavily. Based on evaporation only the maximum operating temperature for lithium would then be about 380 °C, while including the ad-atom model could make this less than 300 °C. Relatively small variations in these parameters can make this loss channel important or unimportant. A recent study with thin Li layers in MAGNUM-PSI indicates that the loss model requires modification due to the formation of LiH under high hydrogen fluxes, which would have different properties than Li [29]. More detailed information on the energy distribution of the impinging ions and neutrals, and the sheath acceleration are also needed to complete a model for losses.

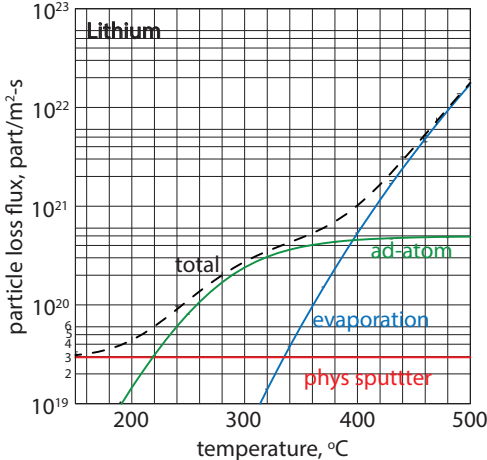


Figure 2. Loss from lithium liquid metal as a function of temperature from physical sputtering, ad-atom loss, and evaporation. This assumes specific ad-atom coefficients.

2.2 Core plasma tolerance for liquid metal species

The tolerance of the core plasma for liquid metal impurities is largely driven by fuel dilution, core plasma radiation, Z_{eff} limitations, and the need to meet heat flux limits in the divertor and minimum neutron wall loads. A coronal equilibrium model is used here [30], and radiation losses include cyclotron, bremsstrahlung and line. The fraction $f_X = n_X/n_e$. For Li ($Z=3$), the FNSF had no operating space since Li does not radiate in the core plasma and the divertor heat load constraint could not be met, or the fuel was diluted so much that the neutron wall load target was not met. If Ar ($Z=18$) was introduced with Li, then solutions ranged from $f_{\text{Ar}}/f_{\text{Li}} = 0.003/0.02$ to $0.0045/0.015$. If Sn ($Z=50$) was introduced with Li, then the solutions ranged from $f_{\text{Sn}}/f_{\text{Li}} = 1.5 \times 10^{-4}/0.037$ to $5.5 \times 10^{-4}/0.027$. For Sn by itself, the maximum fraction in the core plasma was 6.0×10^{-4} and was limited by a maximum Z_{eff} of 2.5, since the lower hybrid, ion cyclotron, and electron cyclotron current drive efficiencies scale as $1/(C+Z_{\text{eff}})$. This Z_{eff} limit determined the maximum Ga ($Z=31$) to be 1.7×10^{-3} , and the maximum W ($Z=74$, used for comparison) of 2.6×10^{-4} . From these limits one can estimate the tolerable loss flux from the liquid metal by scaling,

$\phi_{LM1,loss}^{max} \sim \phi_{LM2,loss}^{max} (Z_1/Z_2)^2$, although this should not be used for Li, since it does not radiate from the core plasma. The tolerable fraction of liquid metal (e.g. $f_{Sn} = n_{Sn}/n_e$) in the core plasma implies a separatrix density, determined by the density profile. Tables 1 and 2 show the various cases, along with other parameters for the FNSF plasma. The maximum values for the impurities in the core plasma can vary depending on the detailed profiles and particle transport, so these can be considered approximate. The analysis of the scrape-off layer and divertor can establish a separatrix density for a given flux source coming from the wall, similar what was done in ref. [28]. The possible segregation of Li to the surface of liquid metal alloys M-Li, indicates that these materials may only release Li while providing a high recycling wall condition, unlike pure Li which would release Li and have a low recycling wall condition. This is discussed further in Sec 2.3. From the evaporation rates shown in Fig. 1, it is clear that Li has a much higher rate than the M-Li alloys.

Table 1. Acceptable lithium and argon, or lithium and tin impurity fractions in the FNSF core plasma.

Ar fraction	0.003	0.0035	0.004	0.0045	0.005
f_{Li}^{max}	0.02	0.02	0.018	0.015	0.01
$P_{fusion, MW}$	509	505	512	505	502
$P_{rad,core, MW}$	49	56	60	67	77
Z_{eff}	2.09	2.25	2.37	2.51	2.81
$H_{98(y,2)}$	0.99	1.0	1.0	1.02	1.01
$\langle N_w \rangle, MW/m^2$	1.18	1.16	1.18	1.15	1.16
f_{DT}	0.84	0.83	0.84	0.82	0.82

Sn fraction	0.00015	0.00025	0.00035	0.00045	0.00055
f_{Li}^{max}	0.037	0.035	0.034	0.029	0.027
$P_{fusion, MW}$	505	505	502	502	509
$P_{rad,core, MW}$	49	70	84	102	116
Z_{eff}	1.63	1.88	2.11	2.34	2.57
$H_{98(y,2)}$	0.99	1.0	1.02	1.02	1.04
$\langle N_w \rangle, MW/m^2$	1.15	1.16	1.16	1.17	1.16
f_{DT}	0.84	0.84	0.83	0.83	0.84

Table 2. Acceptable tin, gallium, argon and tungsten impurity fractions in the FNSF core plasma.

	Sn (Z=50)	Ga (Z=31)	Ar (Z=18)	W (Z=74)
f_{Li}^{max}	0.0006	0.0017	0.0049	0.00026
$P_{fusion, MW}$	516	536	516	560
$P_{rad,core, MW}$	115	72	63	186
Z_{eff}	2.53	2.45	2.50	2.46
$H_{98(y,2)}$	1.02	0.99	1.00	1.03
$\langle N_w \rangle, MW/m^2$	1.19	1.23	1.19	1.28
f_{DT}	0.91	0.90	0.87	0.93

2.3 Segregation of the low surface tension constituent in a liquid metal alloy

The segregation of one constituent to the surface of a liquid metal in an alloy (M-Li) is driven by the surface tension, and the constituent with the lower surface tension will move to the free surface. This is not a large-scale separation of the two components, but only involves several monolayers near the surface, while the bulk liquid metal retains the stoichiometry of the alloy (e.g. 80% Sn and 20% Li). There are other forms of segregation, such as gravity in the case of heavy and light components, but this will not persist if the liquid metal layer is not flat with the surface facing upward. The physics of surface tension and segregation has been studied outside of fusion for some time. A particularly good theoretical analysis of segregation for NaK liquid metal is given in [31], using a detailed variational construction and a density profile trial function. This analysis shows the density profiles for Na and K in the vicinity of the liquid metal surface, clearly showing the K density exceeding that of Na on the surface over a range of fractions of K in Na, and even as the fraction of K drops very low (~2%), the K is localized to the surface has equal density as Na. A strong experimental reference is [32], where a significant reduction in surface tension with segregation is observed with Sn added to Cu or Ag, and where a thermodynamic formulation, with Butler's equation, is used to estimate the surface tension and segregation properties. This phenomena is evident in many alloy systems, and has been suggested for Sn-Li [33, 34], however, a detailed understanding will be needed to project the performance of this alloy to fusion conditions. Interesting and potentially beneficial properties have been observed or postulated for Sn-Li including 1) Sn does not appear to be physically sputtered, only Li [21], 2) self-sputtering of Sn reaching unity is avoided [21], 3) uptake of hydrogen is limited [35] unlike pure Li, and 4) Sn-Li has a much lower evaporation flux than Li. Concerns with establishing and sustaining the segregation effect includes 1) weakening with increasing temperature, 2) the speed with which this segregation is established versus mixing or other fluid disturbances, 3) formation of LiH in the segregated layer, 4) and how impurities in Sn-Li could affect the segregation. Meanwhile Pb-Li appears not to form a segregated Li surface, or only a weak one [36]. Earlier work [37] had confused gravitational segregation with surface tension segregation, which was pointed out in [36]. The surface tensions of Pb, Sn, Li, In, and Ga are shown in Fig. 3 along with Pb-Li.

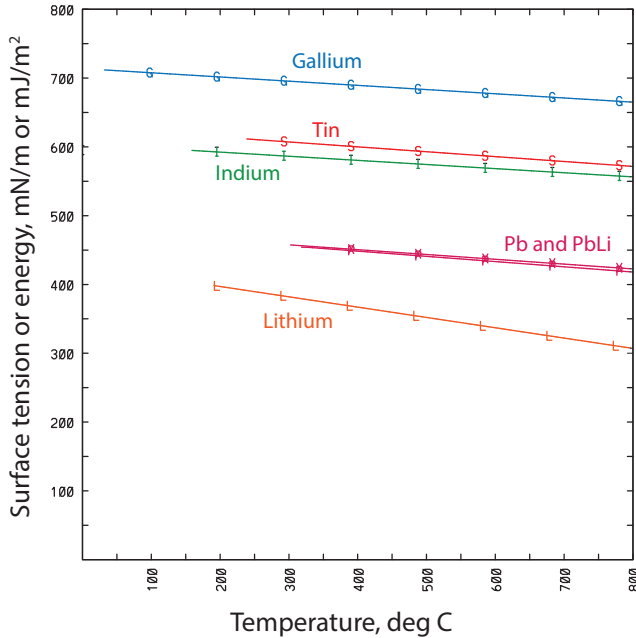


Figure 3. Temperature dependence of the liquid metal surface tension above their melting temperature for various liquid metals.

2.4 Lithium-hydrogen phase diagram

The Li-H (Li-D and Li-T) interaction is critical in a fusion reactor where large fluxes of hydrogen will contact the liquid metal regardless of the particular concept used, either on the first wall or the divertor, although the fluxes can be quite different in these two regions. For liquid metals (e.g. Sn, Sn-Li, Pb-Li) other than Li, the interaction appears much weaker since their hydrogen solubilities are considerably lower than pure Li, although this requires more detailed confirmation. The Li-H or Li-LiH phase diagram (T vs. composition) can be found in [38,39], while p vs. composition can be seen in [40,41], with the full data accumulation for Li-H, Li-D and Li-T in [42]. The phase diagram, temperature versus hydrogen fraction shown in Fig. 4, shows six major regions; 1) the solid Li and solid LiH at $T < 180$ °C, 2) the lower hydrogen content (Sieverts region), liquid Li from $T > 180$ °C, 3) the liquid Li and solid LiH, $T < 685$ -690 °C and H fraction $>$ solubility limit, 4) the liquid Li and liquid LiH, $T > 685$ -690 °C and H fraction $>$ solubility limit or H fraction $<$ upper solubility limit, 5) liquid LiH with very low Li, $T > 685$ -690 °C, H $>$ upper solubility limit, and 6) liquid Li and H, $T > 960$ -1000 °C, where LiH decomposes. Apart from avoiding solidification of a Li-LiH liquid metal solution, the all solid region is not of interest. Above the melting temperature of Li, there is the lower hydrogen content region in which Li is a liquid and either hydrogen is dispersed in the liquid, or LiH is dispersed in the liquid. In this region adding hydrogen to liquid Li can continue until the solubility limit is reached with hydrogen remaining in solution, after which adding more hydrogen LiH will precipitate out as a solid in solution if $T < 685$ °C, or as an immiscible (does not mix) liquid if $T > 685$ °C.

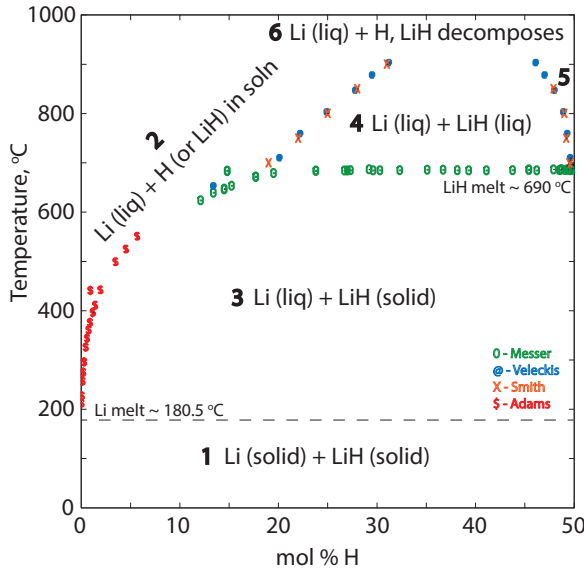


Figure 4. Phase diagram data for Li-H (Li-LiH), Messer [43], Veleckis [40], Smith [41], and Adams [38].

Assuming a flowing Li first wall concept and that all impinging hydrogen is heldup, one can calculate if the Li will reach the solubility limit while in the plasma chamber, as a function of the thickness, flow speed and temperature. This is shown in Fig. 5, for three different particle fluxes ranging from 10^{23} to 10^{25} part/m²-s, for a flow length of 0.76 m typical of a divertor surface in the FNSF. Flow speeds range from 1 to 10 m/s, and the LM layer thickness ranges from 1 to 10 cm. The higher particle fluxes and lower flow speeds lead to the highest hydrogen concentration and depending on the temperature can exceed the solubility limit and lead to LiH precipitation. The hydrogen particle fluxes are lower on the first wall than in the divertor, and even though the flow paths tend to be longer than in the divertor, the uptake of hydrogen did not reach solubility limits. It is important to note that the low flow speeds (< 1 m/s) and thin LM layers (< 1 cm) will lead to the greatest potential for hydride formation and precipitation. Concepts that have very thin layers, and very slow flow (not shown on the graph in Fig. 5) could be susceptible to this effect. The formation of solid LiH in solution can lead to deposition on solid surfaces along its flow path, including outside the plasma chamber on various manifolding.

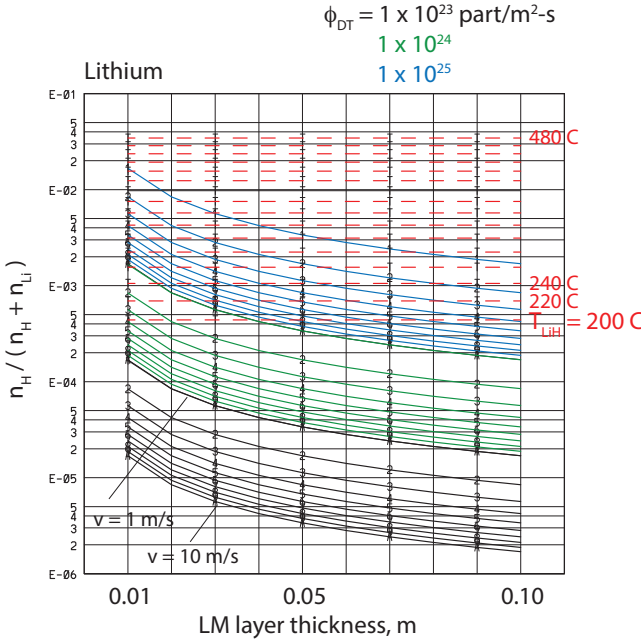


Figure 5. Variation of the hydrogen fraction in Li-H as a function of liquid metal thickness and flow speed, and DT particle flux to the Li surface. Solubility limit is noted by red dashed lines for various temperatures.

The region with the hydrogen content exceeding the solubility limit, with $T < 685$ °C, is a combination of liquid lithium and solid LiH. In a working system of a liquid metal PFC, the presence of a solid in solution can lead to precipitation out onto solid substrate or piping surfaces. Meanwhile the temperature range of liquid Li has typically been set roughly at < 400 °C due to high evaporation rates, where the solubility limit of hydrogen is about 1.2 atomic %. In this region extending from $T \sim 180$ -900 °C, when the hydrogen is less than the solubility limit, does Li with H in it evaporate at the same rates as pure Li? Furthermore, when the hydrogen content exceeds the solubility limit, is the Li evaporation rate the same or different from pure Li? The Li evaporation rate could simply be a weighted value based on the amount of free Li in the Li-LiH mixture. Understanding the properties of the Li-LiH mixture is needed to properly assess evaporation rates and the operating temperature range, as well as solid precipitation potential. The presence of LiH could significantly alter other processes including physical sputtering and ad-atom losses, wetting, and segregation. There may even be a higher temperature operating regime for a liquid metal mixture of Li and LiH, for example ~ 800 -1000 °C, where Li and LiH are liquids, or where Li and H coexist. This would be dependent on the evaporation rates in these regimes. For example, evaporative divertor concepts like the vapor box divertor concept [44-46] relies on lithium operating at ≥ 700 °C, where evaporation is very strong, decreasing to ~ 300 °C, across the divertor length, where condensation should dominate over evaporation. The different regions of the divertor would be in different regions of the phase diagram depending on their operating temperature, pressure, and hydrogen concentration.

2.5 Wetting of liquid metals on substrate materials

Wetting of a solid surface by a liquid refers to its ability to adhere to the surface, and directly reflects an interaction between the liquid and solid. This property is measured by a contact angle, often experimentally measured with a drop of liquid on a surface or a solid plate dipped and removed from a liquid bath. This angle is between the solid surface and the liquid surface at the contact point, with $> 90^\circ$ referred to as poor wetting and $< 90^\circ$ referred to as good wetting. Wetting is strongly complicated by practical features of the liquid and the solid. Surface roughness, solid constituents, solid impurities, liquid constituents, liquid impurities, temperature, and time all contribute to the final wetting behavior [47-50]. Here the difference between a high purity laboratory measurement and an industrial liquid metal flow system are tremendous. Wetting has also been studied outside fusion extensively with some applications being underground oil wetting of rock, soldering, coatings, bonding metals to ceramics, brazing and joining, melting and casting, and construction of composite materials. Good wetting is fundamental to capillary liquid metal concepts, both in feeding the liquid metal from a reservoir to the plasma-facing surface, but also for adhesion of the liquid metal to the substrate surface, which is often a mesh or non-smooth structure. One of the most important aspects of wetting is the interaction between the liquid metal and the substrate material, which tend to enhance wetting. For example, the formation of interlayers between the solid substrate material and the liquid metal can substantially improve wetting, even for systems that originally had poor wetting [49]. This was observed to occur over time with the duration shortened by higher temperatures. In addition, the interlayers were different based on impurities in the solid substrate. These phenomena are interconnected with corrosion [50]. A recent experiment on wetting of liquid lithium on several materials as a function of temperature [51], showed the impact of surface conditions, and that Li wets itself very well (it is well known that a material will wet itself). Excepting capillary systems, why does wetting matter? For flowing liquid metal systems, is wetting actually important? Theoretical work in [52] examined the impact of finite slip, associated with poor wetting, at the conduit walls in duct flow, and found that this condition led to less drag and lower projected pressure drops. The implications for free-surface flow have not been analyzed. Heat transfer examinations in [53], indicated that the convective heat transfer coefficient was only reduced by 10% in a finite slip situation compared to the typical no-slip condition. In a fusion reactor, which is really an industrial scale system, a liquid metal PFC system may transiently experience mediocre wetting, however, the inevitable interactions like corrosion or infiltration could improve wetting quickly, depending on the material substrate. In fact, this is a common observation for sodium (Na) flow in ducts [54] where the observed flow velocity is higher initially when oxide layers are present inside of piping, but the velocity drops as the oxide layer is worn off and the Na wets the pipe walls, because it is interacting with the pipe wall material. Wetting studies will need to move past basic studies and approach the prototypical conditions to make relevant conclusions for LMs in fusion devices.

2.6. Hydrogen uptake in liquid metals

The uptake of hydrogen (D and T) inside the plasma chamber as the liquid metal is in contact with the scrape-off-layer and divertor is important in order to understand its impact on plasma operation as well as its handling for tritium outside the fusion core. It is well known that lithium can retain hydrogen up to 1:1 Li:H ratio [55], and that uptake from a plasma environment can be very strong. Since the mobility of hydrogen is high in

liquid lithium, hydrogen can continue to be absorbed up to this limit of one hydrogen atom per lithium atom. Recent experiments on thin films of Li on MAGNUM-PSI [29] indicate that this is a credible scenario, and it was necessary to reformulate loss analysis to consider LiH as a significant fraction of the exposed LM. As mentioned in Section 2.4, thin Li films that move slowly are particularly susceptible to a high level of hydriding. There are several reports of the positive effects of lithium on plasma facing surfaces in confinement devices for the performance of plasmas. Most of these are associated with a pumping effect of the scrape-off layer by the lithium [56-60], and subsequent changes in the edge plasma conditions. A recent report indicates that in the particular case of Li on carbon surfaces, Li may not be acting as the absorber of hydrogen [61], but actually oxygen is providing the hydrogen uptake. Careful attention to the surface chemistry is critical to uncover the plasma and PFC interactions.

Several experiments have been performed to determine uptake of hydrogen by Li, by using thermal desorption after a Li sample is exposed to hydrogen gas or plasma [62, 63] that can be complicated to interpret. It appears that the difficulty with virtually all of these experiments is likely the presence of oxygen. Even extremely small amounts of water can bring in a level of oxygen sufficient to alter the chemistry at the surface, and near surface layers of liquids and solids. The presence of Li_2O and LiOH at the surface of bulk Li or LiH create chemical reactions that cause desorption of hydrogen at temperatures that would be hard to understand based on the phase diagram of Li-H alone [65]. Ref. [65] shows the chemical reactions that are likely responsible for the observed desorption of hydrogen from Li and LiH samples, which actually involve LiOH , Li_2O , Li, and H. This will require further investigation to understand the role of impurities like O in the Li and H interactions.

The deuterium uptake was measured in ref. [35] for Sn and SnLi, using LM samples exposed in the ISSTOK tokamak. The apparatus was carefully constructed to allow preparation of the samples and plasma exposure within the same enclosure, controlling the impurities on the sample surfaces. Nuclear reaction analysis was used rather than thermal desorption and indicated that retention fractions ($n_{\text{D}}^{\text{retained}}/n_{\text{D}}^{\text{incident}}$) were approximately 3×10^{-4} for Sn, and 2×10^{-4} for SnLi, showing very low retention typical of solid PFCs like tungsten.

2.7 Impurities in Liquid Metals

Impurities are a common occurrence in LMs, and they are normally separated into intrinsic impurities and extrinsic impurities. The former generally arise from the mining or recovery of the ore, processing of the material, and also the tendency of the LM to absorb environmental elements from air in the process of use or preparation, for example. Li has well-known primary intrinsic impurities of O, C, and N. Extrinsic impurities would be those introduced in a specific application, so corrosion products from interactions with the substrate materials, plasma species (D, T, He, Ar, etc.), piping materials, and heat-exchanger materials. Impurities in LMs can alter their behavior and properties significantly, such as wetting, segregation, and surface tension. For example, although corrosion of steels by Li is weak, this is only true if the N level is kept below 10-50 wppm [65]. For values above this the corrosion can rapidly become more aggressive. A present application of Li on a large scale is the IFMIF fusion neutron

source development [66]. Here the Li loop, which does not have a magnetic field, has been devised to have a significant cleanup system to remove N, O, and C, as well as tritium. One of the few examples of detailed impurity identification was done in ref [67], for the alloy Sn-Li, as part of an effort to fabricate this alloy for use in research. It is important for the LM PFC community to begin characterizing the LM's composition, particularly the impurities in these LM's on a routine basis. Early studies in LM's, during the 1950's and 60's, were plagued by different impurity content among LM experiments making the correlation of results very difficult. Naturally this includes surface contamination in a wide range of experiments with free-surface LMs.

The corrosion products in a LM can be picked up in the piping or other apparatus (heat exchanger) outside the fusion core or in the fusion core. The impurities present in the fusion core will be exposed to neutrons and can experience transmutation to new radioactive impurities. Ultimately the various impurities in the LMs must be removed with specific cleanup approaches. Knowledge of the corrosion products produced, their concentrations in the LM loop, including the plasma facing part, is important to predict the various species present and devise clean-up techniques to remove them. At least initially knowing the solubility data for the various impurities in the LM is critical to understanding their tendency to remain in solution or precipitate out, as well as the temperature dependence of this behavior. However, there are many compounds which can form in the LM among the various impurities complicating the treatment significantly. An interesting example of the complex impurity issues can be seen in ref. [68], where the liquid metal Hg is used as a target in a spallation neutron source, and must deal with the wide range of impurities produced by nuclear reactions as well as the inherent impurities in the Hg, their subsequent behavior in the system, and finally their removal by techniques that are known in some cases and undeveloped in others. Once the chemistry of the impurities is understood, there may be motivation to remove specific impurities from the LM or their sources from the LM loop in order to avoid severe issues with its behavior.

3.0 Nuclear aspects of liquid metal candidates

The plasma facing liquid metal will experience the direct neutron flux from the plasma, and its impact on tritium breeding is critical. Initially a wide range of liquid metals were examined by taking a liquid metal PFC thicknesses of 0.1, 1.0, and 10.0 cm, followed by a thick breeding material section. This was done with 1D nuclear analysis, and reported in ref [5]. The breeding zone was a homogenized representation of the DCLL blanket for the FNSF [69]. Combinations of the liquid metal PFC / liquid metal breeder were examined (e.g. Sn/Sn-Li, Sn-Li/Sn-Li, Pb/Pb-Li). Both the Li fraction in the liquid metal alloys and the Li-6 fraction were varied for the breeder zone as well. The neutron multiplication properties were generally similar for Pb, Sn and In, and much lower for other low melting point metals. The tritium breeding ratio (TBR) was only significantly greater than 1.0 when Pb-Li was the breeder, Sn-Li was found to be a marginal breeder which is consistent with ref [70]. Liquid metal PFC materials that worked best with a Pb-Li breeder were Li, Pb, Pb-Li, and Sn-Li. On the other hand, if the liquid metal PFC is very thin, such as 1 mm thick, virtually all the liquid metals will perform similarly with Pb-Li as the breeder.

In order to understand the benefit of having a liquid metal layer on the first wall in terms of reducing the neutron damage and He production, Li, Sn, and Pb-Li were considered as liquid metal PFCs. The thickness of the layer was varied from 0 to 30 cm, with a solid substrate assumed to be behind it. Although there were slight differences among the PFC materials, overall it required about 10 cm's to reduce the displacements per atom (dpa) by 2.5 times, and about 16 cm's to reduce it by 5 times. Although these results show that the nuclear damage of solids is not strongly reduced without going to thick liquid metal layers, a 5 cm thick layer could reduce the peak dpa by 1.67 times, and a 2.5 cm would yield a 1.25 times reduction. Since the He and H production are also neutron energy dependent, the reduction would be somewhat stronger.

Specific activities and decay heat show that Pb, Ga, and Li (assuming tritium is removed) are superior with rapid fall off over one day to one week, and continuing to one year. Indium starts high and only decays slowly, while Sn decays only slowly, with a little more than 10 times reduction after one year. The penalties of specific liquid metal PFC materials will be dependent on volume and the potential to separate the activated impurities and transmutations from the liquid.

More detailed analysis with 3D MCNP was performed with models of a FNSF sector [5] with no penetrations. The liquid metal thickness was fixed at 2.5 cm, based on simulations of flowing LM concepts [8], in front of a collapsed version of the same RAFM substrate material of 34% MF82H + 67% He that made up the first wall of the FNSF design, and all cases have Pb-Li as the breeder. The LM's examined were PbLi, Li, Sn, and SnLi. Lithium was taken to be 90% enriched in Li-6 in all cases. The presence of the LM increased the tritium breeding ratio in all cases above the reference by 4-13%, the highest being Li due to direct breeding, and Sn the lowest since its only providing additional neutron multiplication. The neutron multiplication is enhanced with Pb-Li, Sn and Sn-Li by up to 14%. Material damage at the substrate solid (RAFM steel) is reduced, compared to the reference, by the 2.5 cm LM layer between 2-10% on the outboard side and 9-15% on the inboard side. Meanwhile He production was reduced in the range 19-35% on the inboard and 9-23% on the outboard. The strongest reductions were from Pb-Li, Sn and Sn-Li dominantly due to neutron multiplication and lowering of neutron energies. Very similar results are seen for the H production. Overall, since the LMs of interest for the PFC application (Li, Sn, and Sn-Li) have strong nuclear reactivity they have an important impact on tritium breeding, material damage and He/H production that must be accounted for, and are sensitive to LM layer thickness. LM PFC concepts that have very thin layers (~ 1 mm) would generally have only weak impacts compared to a case with no LM PFC, and the differences between liquid metals would be minor. Ref [5] should be consulted for the detailed assessments.

4.0 Solid substrates for liquid metal PFCs

The liquid metal concepts examined in this study will all have some form of a solid substrate to support the liquid metal. This may be a first wall surface, a base and mesh on the first wall, a divertor flow surface, or divertor base and mesh, or tubs in the divertor, all connected to a helium cooling system similar to the breeding blanket or traditional solid divertor concepts. The interactions between the liquid metal and the solid are clearly critical, however, the database on liquid metal / solid interactions ranges from 30-

60 years old, and often involves materials that are not fusion relevant [71]. Recent work [72, 73] shows both the importance of developing a materials loss rate (kg/yr or mm/yr) for each liquid metal/solid combination, and carefully diagnosing the liquid-solid interlayers in order to know the long-term conditions that will develop in steady state. Pursuing reduced activation ferritic martensitic (RAFM) alloys, and their variants, is important for fusion since there are no other alternative structural materials sufficiently mature to compete. On the other hand, it is well known that a number of refractory metals have good compatibility with a wide range of liquid metals (e.g. Mo, W) at high temperatures [74, 75]. This must be balanced against avoiding high nuclear activation materials, generally restricting their use to coatings on RAFM for example.

Reviewing the corrosion data for Li, Sn, Sn-Li, and Pb-Li it can be seen that Li has low corrosion rates in contact with steels, and it is even lower with ferritic steels than stainless steels. The best data comes from the 1980's [76-85] and some earlier data summaries [86]. These experiments involved both thermal and forced convection loops. Up to temperatures of 500-600 °C, the thinning rate is $< 0.0025\text{-}0.025$ mm/yr, over a wide range of flow velocities. Experiments do show higher initial material loss rates before relaxing to the slower thinning. The control of intrinsic impurities (O, N, C) in Li is critical to obtaining these low corrosion results, and the technology for this has largely been established. IFMIF represents the latest research into fast moving liquid Li, however the effect of a magnetic field on lithium corrosion has not been established. For comparison, extensive corrosion studies have been done recently for Pb-Li since it is a primary blanket breeder candidate. Static corrosion tests for Pb-Li and RAFM steel showed ~ 0.04 mm/yr [84-86], and forced convection flow at 10-20 cm/s showed ~ 0.2 mm/yr [87-89]. The forced convection in a magnetic field then resulted in $\sim 0.3\text{-}0.4$ mm/yr [90-92]. These thinning rates for Pb-Li are not acceptable, since they could result in structural failures in too short a time frame, and will require amelioration. Tin shows a more rapid corrosion rate than does Li, and in general Sn-Li has similarly rapid corrosion. Static corrosion tests [93, 94] resulted in $\sim 3\text{-}15$ mm/yr thinning for both ferritic and austenitic steels exposed to Sn, and also shows a strong increase in corrosion rate as the temperature rises from 300 to 700 °C. The refractory metals W and Mo have good corrosion resistance to Sn even up to > 900 °C [95]. Whether these could be used as sustainable coatings is unclear. In contrast, the use of Al additions to steel, which forms a self-sustaining alumina layer, has been shown to be effective at reducing the corrosion in high Cr ferritic steels [96] exposed to Pb-Li, and aluminide/alumina layers show potential as well [97]. Finally, for Ga the corrosion rates [98] for steels are enormous, ranging from 30-50 mm/yr for temperatures of 400-600 °C, and largely eliminates this liquid metal as a candidate, as noted in Section 1.

In addition, MHD in the liquid metals, or currents intentionally driven in the liquid metals, likely require insulating layers in order to reduce large drag and pressure drop. The use of electrically insulating materials in contact with the liquid metal significantly reduces the pressure drop (resistance to flow) compared to conducting walls, by forcing the currents generated in the conducting liquid metal, as it moves through a magnetic field, to return through the fluid and produce a balanced body force over the whole cross-section. These can take the form of an intrinsic layer [84] (Al_2O_3) that forms on its own, an insulator coating applied on RAFM steel, or a fully solid ceramic structure (e.g. SiC-SiC composite). These layers would be in close proximity to the plasma and neutron

fluxes, and their sustainment and ability to provide this insulating function requires verification. It should be emphasized that insulating flow paths for LM's are required anywhere the magnetic field is significant, and also in the fringing field outside the main magnets (toroidal and poloidal field coils). For a first wall or divertor application where high flow speeds are required, the injector apparatus would need to have insulation, and might even be entirely constructed of insulating materials. The compatibility of LMs with various insulating materials is not well understood except in some particular cases (e.g. alumina and PbLi) and require significantly more development.

A serious failure mode for liquid metal and solid combinations is often called liquid metal embrittlement (LME, or many other names). In this situation the liquid metal can rapidly penetrate a solid and severely embrittle it, allowing rapid crack propagation in the solid when it is under tensile stress. Any liquid metal / solid combination must be shown not to be susceptible to this mechanism before it can be accepted for application in a fusion reactor. This could be dependent on impurities in the liquid metal, as well as the solid. Although this mechanism has been recognized since the 1950's it has only obtained an empirical understanding. Difficulties arise due to different mechanisms for embrittlement, different rates of embrittlement and sensitivity to environmental conditions. There are well known LME pairs such as Al-solid and Hg-liquid, stainless steel-solid and Zn-liquid, and steel-solid and Cu-liquid. There are a wide range of related processes including stress corrosion cracking, corrosion fatigue, and hydrogen embrittlement. There is an enormous literature on LME, some older references discussing observations include [99,100], some attempting to coordinate observations [101], and some recent efforts can be found in [102,103], although these are hardly exhaustive. Attempts to develop predictive models have generally suffered from numerous counter-examples that can be found in the experimental literature. It is critical to develop a reliable and accessible experimental process for identifying susceptibility for a given application (which would include normal and off-normal operation parameters). For example, if an accident resulted in the spilling of the liquid metal onto the vacuum vessel, the liquid metal – vacuum vessel solid combination would also require clearing against LME (in addition to the PFC substrate solid material), and at a wide range of temperatures and stresses.

5.0 Integration Issues with Liquid Metal PFCs

The application of liquid metals to the plasma facing region requires the integration of the system into the fusion plant. A simple view of this system is shown in Fig. 6, which represents the loop over which the liquid metal is exposed to the plasma producing the hot leg, which proceeds through the tritium (and deuterium) extraction apparatus, then through a heat exchanger producing the cold leg, then through a clean-up apparatus (or multiple), and finally through an apparatus to re-establish its desired constituency (e.g. 20% Li and 80% for $\text{Sn}_{80}\text{Li}_{20}$).

The liquid metal would begin at the constituency control where it is established to have the correct stoichiometry, Li-6 enrichment, and minimized impurities (irreducible impurity levels) in the cold leg. When the liquid metal enters the plasma region it will pick up D, T, He, Ar (radiating impurity), corrosion products from solid substrate materials, and will contain transmuted isotopes of its constituents, corrosion products,

and irreducible impurities. The LM receives its heating from the plasma as a surface and a volumetric heat load. After exiting the plasma region it should first encounter the tritium (hydrogen) extraction systems where the hydrogen isotopes are removed. This extraction apparatus will depend on the specific LM. The piping that provides the liquid metal loop can introduce additional impurities depending on what it is made of and the temperature and flow velocity. The liquid metal will then reach the heat exchanger where its temperature will be reduced, and additional impurities can be introduced from the HX materials. The cold leg of the loop begins after the heat exchanger and proceeds to the clean-up systems, which is likely to be composed of a series of separate actions to remove specific types of impurities (e.g. magnetic traps, cold traps). The liquid metal then moves to the constituency control where the main liquid metal components are balanced, Li-6 is enriched to enhance breeding if necessary, and intrinsic (O, N, C) and trace impurities are introduced with the liquid metal components. In order to model the liquid metal loop one requires a energy balance for the liquid metal as a whole, and a concentration balance for all constituents and impurities, presented here in a lumped parameter simplified system to demonstrate the sources and sinks.

$$\rho C_p \frac{dT}{dt} = \nabla \cdot (k \nabla T) + v \cdot \nabla T + S_{\text{plas}}^{\text{surf}} + S_{\text{nucl}}^{\text{vol}} - L_{\text{heat}} + h_{\text{HX}} \Delta T + h_{\text{clean}} \Delta T$$

$$\frac{dC_i}{dt} = \nabla \cdot (D \nabla C_i) + v \cdot \nabla C_i + S_{\text{plas}}^i + S_{\text{subs}}^i + S_{\text{irrad}}^i + S_{\text{piping}}^i + S_{\text{HX}}^i - E_{\text{clean}}^i + S_{\text{constituency}}^i$$

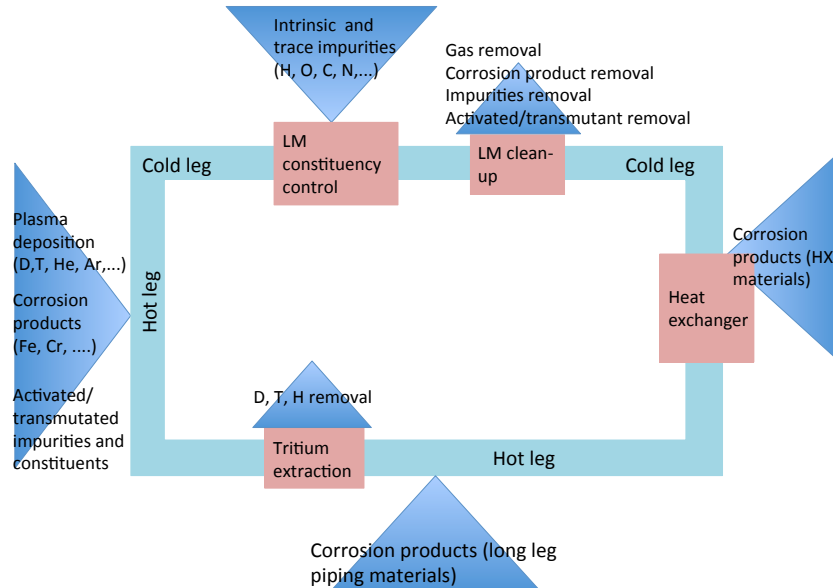


Figure 6. A simplified LM PFC flow loop in the fusion plant.

It should be noted that although one might assume velocity profiles for simplicity, there are momentum equations that would accompany these that would provide those profiles, and more importantly they would show flow effects that could lead to deposition or other phenomena (e.g. pipe expansions). In addition, boundary layers would be prescribed for flow velocity and mass transfer more consistently. Chemical reaction equations would

also be included to account for formation of compounds and their reaction kinetics. Here T is the bulk temperature of the LM, S represent heat sources and L represent heat losses, and h are heat transfer coefficients, k are heat conduction coefficients, C_i is the concentration of a given impurity species, S are impurity sources, E are extractions (losses), and D_i is a diffusion coefficient for impurity species i . Corrosion models [104] can be applied based on the mass loss/gain processes at work in a given region. The temperature will dictate the precipitation of compounds formed in the LM, and any chemical reactions, and therefore the possibility of deposition on pipe walls or other surrounding structures. The temperature range around the loop is constrained by major requirements, 1) avoid excessive fluxes from the liquid metal into the plasma region (depending on FW or divertor), and avoid all solidification or precipitation in the loop, with the exception of the clean-up system which may utilize “cold trap” features. In addition, there may be other impacts such as the solid-liquid material interface limits (corrosion). Due to the liquid metal loss limits before impacting the core plasma excessively, discussed in Sec. 2.1, the temperature rise from the liquid metal inlet is restricted. This would affect the flow speed, length of flow path, and liquid metal thickness.

These loss limits are not known accurately, so for Li, Sn-Li, and Sn they can be approximated by using the flux and edge plasma density correlations developed in ref [28] for discussion. Li was identified to allow a loss flux of $\sim 2 \times 10^{20} /m^2\text{-s}$ under low recycling, while $\text{Sn}_{80}\text{-Li}_{20}$ was determined to allow a flux of $\sim 3 \times 10^{18} /m^2\text{-s}$ under high recycling. The corresponding temperature limits associated with evaporation were $\sim 380 ^\circ\text{C}$ for Li and $\sim 540 ^\circ\text{C}$ for Sn-Li. Using the fluorine result from ref [28], and the scaling from section 2.2, the tolerable flux of Sn would be $\sim 1 \times 10^{16} /m^2\text{-s}$, with high recycling, which implies a maximum temperature, based on evaporation only, of about $680 ^\circ\text{C}$. These values ignore the ad-atom processes that might be more limiting.

The tritium extraction is typically done as soon as possible, after the LM leaves the fusion core, in order to avoid higher tritium concentrations in the rest of the loop (e.g. heat exchanger), although it could be part of the cleanup system if the LM is not being used for thermal conversion to electricity (no heat exchanger). The pipe runs throughout the loop would be a source for corrosion products and should be chosen to be very similar materials to the substrates in the plasma chamber in order to avoid longitudinal (along flow path) mass transfer associated with different materials. If the LM substrate materials in the plasma chamber are made of an RAFM steel, then the pipe runs could be made of T91 [105], which is a ferritic steel with very similar constituency, but is much less expensive and is an industrially available material. If there is a heat exchanger in the LM loop, it may be more difficult to choose a material that is very similar, since the HX uses optimized heat transfer metals/alloys, but interactions can be minimized. The cleanup system is critical to the viability of the LM loop and must remove a wide range of materials from the LM including gases, oxides and other compounds, inter-metallics, materials in solution, and radioactive transmutations. Similarly a wide range of approaches are used to isolate these impurities to facilitate removal, including 1) solubility/temperature dependence to create precipitation, 2) raising temperature to invoke decomposition of compounds, 3) mixing with substance that has a higher affinity for the impurity that the LM, 4) centrifugal separation of high mass impurities, 5) liquid/gas interface to allow the escape of gases, 6) slag skimming for cleaning off

naturally separating impurities, and 7) filters to catch precipitating materials in the LM and so forth. A sequence of cleanup schemes is clearly needed and is dependent on the LM. Finally, the LM reaches the constituency control section where new LM is added and temperature returned to its inlet value before proceeding back into the plasma chamber.

5.1 Design windows for plasma-facing liquid metals, and thermal conversion to electricity

The use of liquids facing the plasma in a tokamak imposes overlapping constraints on operating parameters such as surface temperature, bulk inlet and outlet temperature, heat flux, total power removed, flow speed and pumping power. These are best described in the form of design windows. Temperature design windows were examined for three possible coolants (Li, Sn, Pb-Li) in three configurations: thin flowing films, thick flowing jets, and wetted walls. Wetted walls, with nearly stationary liquid films were found to behave very similar to coated solid surfaces. Heat must conduct into an actively cooled substrate. The main concern for these designs is to maintain acceptable surface temperature to prevent excessive contamination of the plasma.

Flowing films are subjected to more complex constraints. Most of our effort focused on divertor applications, which have short exposure lengths (and times) with expected peak local (time-averaged) heat flux in the range of 5-15 MW/m². Temperature rise and flow speed were chosen as the primary axes for representation of the windows, and parameters from FNSF [27] were used to establish the nominal design conditions (e.g. the power levels and nominal plasma footprint).

In Fig. 7 are shown results for 1 cm thick flowing Li, Sn, and Pb-Li in the divertor having a 4.3-cm footprint of heat flux of 10 MW/m². The flow length is 1 m, field is 7.5 T, and the slug flow is assumed with insulated Hartmann walls. The inlet temperature of the LM's are all 350 °C to be compatible with the lower temperature limit of RAFM steel. Figure 7 shows the exit surface temperature (solid, and near surface values) and exit bulk average outlet temperature (dotted, at 3 location in the liquid layer) as a function of LM velocity. The blue box at the left is a constraint imposed by inertia and MHD body forces: higher velocities are required in order to ensure the coolant does not stop within the 1-m length of the exposed surface. (Note, the variation in film thickness due to slowing was not considered in this simplified analysis). The orange box at the top is a constraint imposed by evaporation into the plasma, assumed to be 450 °C, 400 °C, and 800 °C for Li, Pb-Li and Sn, respectively, for this examination. In all cases the bulk average temperature rise of these flowing films is extremely low. This influences the power cycle and pumping power required to maintain the flow (relative to the total power removed). Relatively high flow speed is required to maintain the surface of the lithium below the evaporation limit. Even without the inertia requirement, speeds in the range of 4-8 m/s are needed. Heat fluxes beyond 15 MW/m² will be difficult to remove. The Pb-Li case is intractable due to the low thermal conductivity (4x lower than Li, 3x lower than Sn) and relatively high evaporation rate (low temperature limit) that assumes Pb would be released. Sn was found to have a wide operating space due to its very low evaporation rate (high temperature limit). Mixing of the LM can improve these results, but previous analysis indicates that in a magnetic field, the bulk mixing of LM's can only improve

these projections slightly, since they result in an equivalent thermal conductivity that is only 2x higher. Figure 8 shows additional cases for lithium at varied heat fluxes of 7.5-15 MW/m².

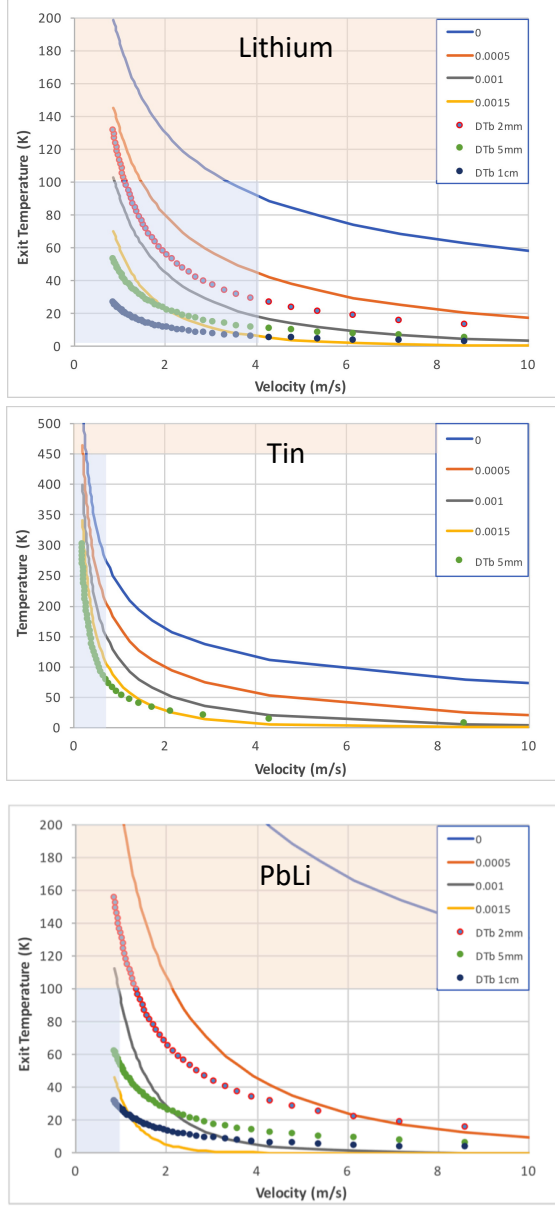


Figure 7. Surface and bulk temperatures of a 1 cm thick LM film flowing over a 1 m long divertor-like surface, subject to a localized 10 MW/m² surface heating. Surface (blue solid) and near surface temperatures (red, gray, yellow solid), and bulk temperatures through the thickness (dotted).

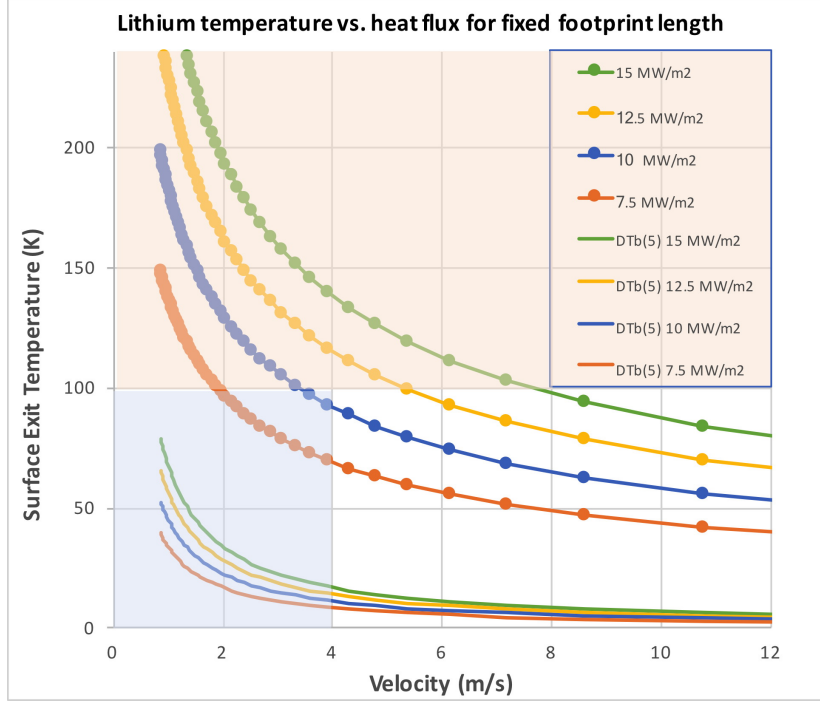


Figure 8. Example design window results for lithium film flow

5.2. Power conversion impacts of using low-temperature PFC's

As much as 20-25% of the total thermal power available for electricity generation, including heating and current drive power injected into the plasma, comes from surface heating. The loss of this energy would be a significant penalty due to both the lost revenue (effectively increasing the COE) as well as thermal waste heat load to the environment. Therefore, integration into the plant power conversion system is desirable.

In recent power plant design studies, exit temperatures from both the blanket and plasma-facing components have been high enough to enable high conversion efficiencies (>50%) using a Brayton cycle, similar to those used today in combined cycle gas turbine plants as well as next-generation fission reactor designs. The impact on conversion efficiency due to temperature constraints imposed by the use of liquid metal divertors were evaluated quantitatively.

Two effects were considered using the ARIES-ACT1 [106] and ACT2 [107] reference power plant design points: the effect of reduction in inlet temperature to the heat exchanger and the effect of reduction in the turbine inlet temperature (i.e., heat exchanger outlet). For a Brayton cycle, the inlet temperature to the heat exchanger has a significant influence on the cycle parameters and can lower the cycle efficiency if the temperature is reduced too far.

Figure 9 shows the effect of a reduction in the heat exchanger inlet temperature on the plant total electric output using ARIES-ACT2 as an example. In ARIES-ACT2, the divertor supplied the highest outlet temperature. If the He/W divertor is replaced by a liquid lithium system, then the turbine temperature will be limited by the blanket outlet

temperature (620°C) instead of the higher value obtained from the He/W divertor (690°C). This was included in the results.

A loss of 125 MW would result from the use of lithium with a heat exchanger outlet temperature constraint of 300 °C. For tin, almost no impact would be seen due to its high temperature capability that nearly matches the operating temperature of ACT2. If a liquid lithium PFC is used in the higher-performing ARIES-ACT1 power core, the total loss of gross electric power is even higher (182 MW). In this case, the loss of electric output is so large that it would be more economic to dump the heat into the environment rather than convert it to electricity.

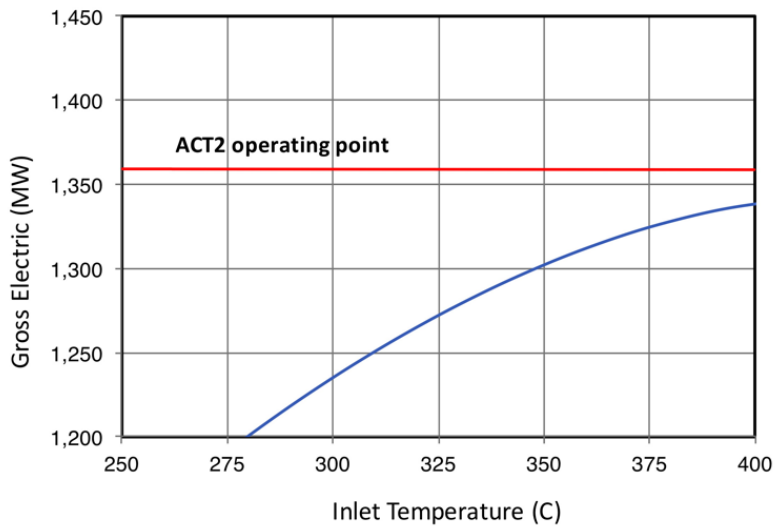


Figure 9. Gross electric power produced by ARIES-ACT2 as a function of heat exchanger inlet temperature. The turbine inlet temperature also was reduced due to the elimination of high- helium from the divertor (which had produced the highest system temperature in ACT2)

5.2. Tritium handling in liquid metal PFCs

The tritium that is produced by nuclear reactions, or implanted in the LM, as it traverses the plasma chamber must be removed or its concentration will build up and create permeation issues throughout the LM loop, and/or inventory issues releasable in an accident scenario. This is particularly acute for Li since it efficiently breeds tritium and has a high solubility for hydrogen (even beyond solubility limits it will continue to absorb hydrogen). Tritium (hydrogen) extraction methods for LMs are in a low state of development although concepts have been studied, and in some cases, small demonstrations have been accomplished. Some techniques for Li include the Maroni process (contact with molten salt), electrolysis, and evaporation/distillation. For most other LMs (with much lower affinity for hydrogen) and even He coolant, the permeator window is considered a primary candidate. Fig. 10 shows a simple tritium flow loop diagram, highlighting the plasma fueling/exhaust and blanket breeding loops. The LM PFC introduces a new fluid to the original system in the FNSF, which contained the blanket He coolant, the divertor He coolant, and the blanket breeder LM (Pb-Li). Each of

these fluid streams requires its own tritium extraction, heat exchanger and cleanup system, based on what the fluid is and also the operating temperature of the fluid.

Attempts to make the PFC and blanket breeder LM's the same material have been difficult. Sn-Li is a poor breeder material compared to Pb-Li or Li, and Pb-Li is unattractive as a PFC material due to the large Z of Pb and higher evaporative losses compared to Sn or Sn-Li. Using Li as the blanket breeder would increase the inventory of Li significantly beyond what is necessary for a PFC application, and the reactivity of Li and its safety implications have largely eliminated it from any blanket concepts being considered presently. IFMIF is the only large scale application of liquid Li, with significant development and prototyping.

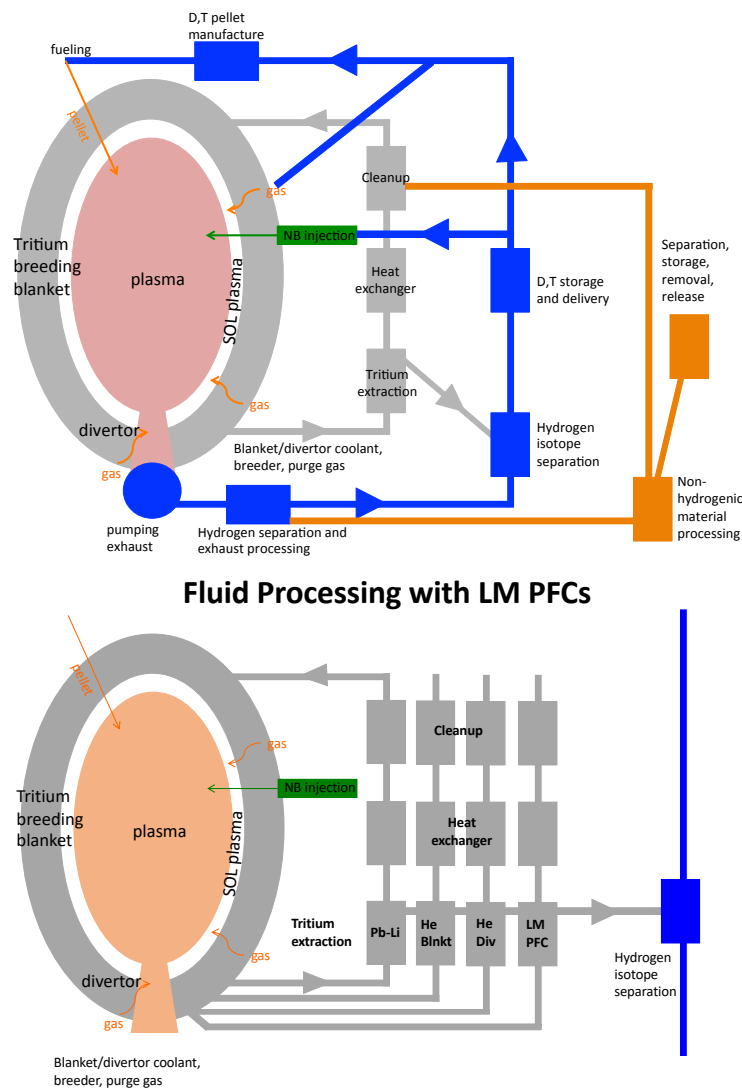


Figure 10. Simplified plant tritium flow loops and expansion of the blanket, divertor, PFC fluid loops showing the need for individual processing for each fluid or operating condition (e.g. temperature).

5.3. Helium pumping from the plasma chamber

Helium pumping with LM PFC systems is generally considered necessary, since it does not chemically bond to any of the LM's nor is it soluble in any of them. This pumping requirement would extend to other gases like argon or neon which might be injected to enhance radiation from the core plasma. Analysis in ref [108], implied that to remove appropriate levels of He to control the core content, the He diffusion coefficient needed to be $< 10^{-8} \text{ m}^2/\text{s}$ to allow reasonable flow speeds of the LM (10's of m/s), for 10 keV incident He ions. Lower He energies would have too shallow a depth of deposition, faster diffusion coefficients would allow the He to reach the surface quickly, and too slow a LM flow would also allow the He to reach the surface before it left the plasma chamber. Another reference [109], subsequently identified the He diffusion coefficient in flowing Li to be $2.5\text{--}6.5 \times 10^{-7} \text{ m}^2/\text{s}$, which would require $> 100 \text{ m/s}$ flow velocity for the highest He energies, or even higher speeds for lower He energies. Although bubble formation or He concentration near the LM surface might lead to a more tenable solution, overall it does not appear that He can be removed by any LM PFC candidate sufficiently well to rely on it to keep the core plasma from diluting, thus requiring pumping of gaseous He. This creates the undesirable feature of also pumping Li vapor for a Li PFC, or smaller amounts of other LM PFC candidates, into the plasma exhaust system simultaneously with the He. Some technique for depositing the Li or other LM, while letting the He pass through will be required.

5.4. First wall penetrations

The first wall and blanket are penetrated by several systems that support the plasma operation, primary of which are the heating and current drive, and diagnostics. The FNSF physics assessment [110] identified $\sim 8 \text{ m}^2$ for NB, LH, IC and EC H/CD access, and $\sim 3 \text{ m}^2$ for diagnostics access. If a flowing LM PFC system is being applied to the first wall, then it must have a way of bypassing the penetration. Specific geometries are likely to be required to minimize disturbing the flow while diverting it around the hole. For some sources (NB) the hole size is a large fraction of a sector area, and different injection approaches might be required. This sort of design and optimization can be addressed in a flowing LM experiment, and requires 3D MHD LM simulations. On the other hand, a capillary system composed of smaller blocks or tailored shapes may have an easier time in accommodating penetrations on the first wall.

The presence of a hole on the first wall, regardless of what is in it, will allow the possibility of LM vapor depositing on the exposed equipment (e.g. straps in an ICRF launcher, waveguides in a LH launcher). The condensation of the LM vapor on surfaces or having vapor in the region can disrupt operation or degrade performance. Depending on the LM, it may be chemically reactive like Li, and form compounds on the structure surfaces. Operating the launching structures at high temperature, which is likely, is a common approach to avoid deposition, although it may increase the power losses in the launcher itself.

5.5 Pumping liquid metals

The LM PFC concepts that introduce the LM into the plasma chamber, by injection or capillary forces, will lose control over the fluid flow. The fluid must be collected and drained out of the plasma chamber largely by gravity and any initial injection force that persists. It has been found in IFMIF prototypes [111] that the LM must be collected into an accumulation tank and sufficient elevation maintained before it can be pumped on, or cavitation will result, and this is now part of the Li systems in the fusion neutron source. This is most easy to visualize for flowing systems. In capillary systems the LM may be allowed to evaporate, or it might be collected and recycled as part of the design. Since the LM adheres to the roughened surface or mesh on the substrate, it will only move if it is overfilled above the height of the irregularity, and the speed of flow would depend on this excess height.

5.6 Magnetic Fields and LM Flow Geometry

Figure 11 shows the basic picture of LM flow over the first wall, which is launched from the top of the device and flows down the walls to the divertor at the bottom of the device, under the influence of gravity and centrifugal (produced by the injection of the LM) forces. In the divertor the LM can land in a tub (full of LM) or it can continue on specifically designed surfaces to guide it to the drain where it leaves the plasma chamber. Focusing on the first wall the geometries of the inboard and outboard surfaces show there is an outward toroidal curvature and an inward toroidal curvature, respectively. There is poloidal curvature only on the outboard. Otherwise the width of a flow path on the inboard is constant, while on the outboard it is narrow, expands and then narrows again. A detailed examination shows the FNSF equilibrium magnetic fields on the inboard, which the conducting LM must flow through. They range from 9.8 to 10.3 T (toroidal field), and 0.0 to 0.06 T (normal field, poloidal field) on the inboard side, and 5.9 to 8.0 T (toroidal field) and 0.0 to 0.15 T (normal field, poloidal field) on the outboard side. These include the plasma and can have up-down asymmetries in the normal field of about ~ 0.01 T due to plasma position. The primary magnetic field is the toroidal field, which is perpendicular to the flow, and simultaneously is perpendicular to the side walls (called Hartmann walls). This is the field largely responsible for large drag on the fluid and the associated pressure drop. The normal field, which is normal to the surface on which the free-surface LM is flowing, is much smaller, but has a significant effect on the flow [8]. The maximum toroidal field ripple is ~ 0.0016 T and the non-axisymmetric field is estimated to be ~ 0.0003 T, both considered too small to affect the LM MHD.

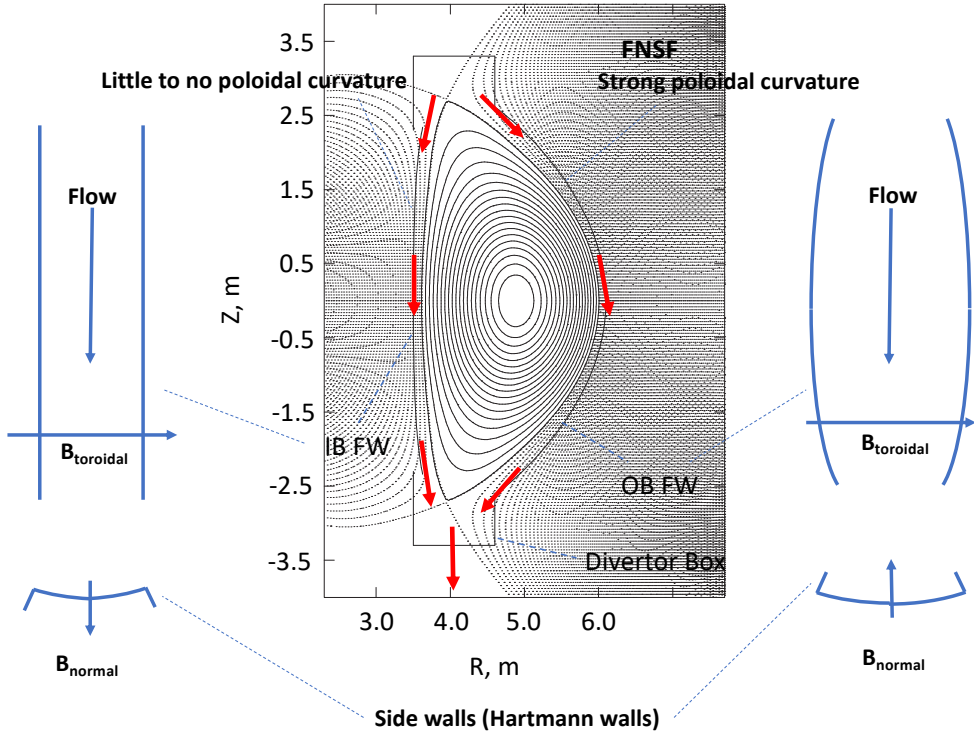


Figure 11. The plasma cross-section with first walls on the inboard and outboard sides. The divertor boxes are also shown. The inboard flow path geometries are also shown, giving the curvatures. Walls are shown for the flow path, which may or may not be present.

Simulations of the flow with MHD fluid and thermal analysis [8] shows that the fluid thickness, flow length, velocity and heat flux all play a role in the design of a flowing system. Here for the first wall the heat flux was low, $\sim 0.2 \text{ MW/m}^2$, to represent the radiative heat flux from the plasma only. The liquid metal, Li in this case, was examined with an entrance temperature of 350°C to observe the lower temperature limit of the RAFM steel substrate. The flow lengths were $\sim 5\text{-}10$ meters in length. Velocities ranging from 1-20 m/s, and initial thicknesses of 0.005 to 0.08 m were examined. In general, the temperature rise was only $30\text{-}40^\circ\text{C}$ allowing Li to stay within its maximum tolerable loss rate (less than $\sim 380^\circ\text{C}$). In addition, the temperature rise was restricted to the outer half of the fluid thickness, only barely affecting the substrate if at all. Clearly higher heat fluxes would require higher velocities. Initially the analysis assumed that the first wall would be toroidally continuous, with no divisions. Under these conditions for the inboard first wall, with a toroidal field of 10 T and a normal field of 0.05 T, the optimum combination was an initial fluid thickness of 0.02 m and an injection velocity of 1.7 m/s, giving a uniform thickness throughout the flow length. This resulted in an allowed temperature rise. Maintaining uniform LM thickness is critical to avoid plasma contact or interference with scrape-off layer flows. In particular, height changes could

allow the LM to receive a much higher heat flux by changing its geometry relative to the magnetic field lines which carry the particles and energy.

On the outboard the situation is more complex with the strong poloidal curvature, and requires higher flow velocities to create a centrifugal force that pushes the LM against the first wall surface. Similar temperature rises, keeping Li within allowable losses, can be achieved with velocities of 2-10 m/s, however maintaining fixed LM height is challenging with the presence of more substantial normal fields of 0.03-0.06 T in these simulations with both varying flow velocity and normal field value. The toroidally continuous case had LM height variations of 2-3 x the initial injected height in the course of the flow down the first wall. The introduction of dividing walls on a sector allowed solutions with significantly weaker thickness variations. This was consistent with maintaining the tokamak since it is necessary to segment the fusion core for removal, and side walls along the edge of the sector could be incorporated. It is important to recognize that the side walls are considered to be electrically insulated, which may be difficult in the first wall location. A comparison of the toroidally continuous and divided wall cases with initial LM height of 0.02 m, and 5 and 10 m/s flow speed, for the inboard and outboard can be seen in ref. [8].

6.0 Technical investigations in LM PFCs

A series of technical investigations were made into areas relevant to assessing the viability of LM PFCs, noted in the Introduction, and some of these are summarized here.

6.1. Tritium behavior and accident scenarios

A variety of tritium transport scenarios in the FNSF using the MELCOR/TMAP model have been examined [4]. This includes the original design with solid FW, and variations with LM PFC's of Li, Sn, and SnLi. The liquid wall model assumes a 1 cm thick FW layer flowing at 10 m/s into a tub-like divertor.

In the solid-wall design, tritium losses from normal operations were similar to our original TMAP model ~23 g/y for 80% efficient extraction from PbLi and ~10 g/y for 90% efficient extraction from PbLi [112]. This is dominated by losses from the pipes in the PbLi cooling system. In all of the liquid metal wall cases, we found that transport of implanted tritium in the FW and its associated loop was essentially de-coupled from transport of bred tritium in the blanket and its associated loops, i.e. the losses from the blanket, SR, VV, and associated piping were essentially unchanged by the presence of the liquid metal FW and divertor.

Additional losses from the FW liquid metal loop piping depend on assumptions about the size of this system as well as the kinetics of implantation and desorption at the plasma/LM interface. For Sn and SnLi, which have low hydrogen solubilities, we have assumed that the desorption process is fast relative to convective transport along the wall [108], and simply scaled the implantation flux by measured retention fractions (~2e-4) for Sn and SnLi exposed to a deuterium plasma [35]. Provided this assumption is valid, losses from the FW loop piping are comparatively small, ~0.01 g/y. For lithium, we assume 100% retention of impinging hydrogen. In this case, it is the inventory in this

loop we are concerned about, assuming it may be released during a fire or other accident. If the extraction system is 70% efficient (single-pass) and this system can be located within 10 m of the vessel inlet/outlet, inventories are kept to ~ 3 g, which is an order of magnitude or so lower than the amount that would result in a dose of 10 mSv to the maximally exposed individual, the limit imposed by the DOE Fusion Safety Standard. Work continues to examine what other consequences a fire of this nature would have, i.e. on heat removal in accidents.

6.2. Edge-plasma modeling for liquid lithium walls

Edge plasma modeling is used to predict the interface behavior between the deuterium/tritium (DT) ions making up the core particle exhaust and the lithium vapor evaporating from the liquid walls [2]. Because the evaporation depends strongly on the surface temperature, the largest lithium source is expected near the divertor plates. A set of steady-state edge plasma solutions are found where upstream, adjacent to the core plasma, the DT ions dominate while in the divertor region, lithium ions dominate, having densities in excess of 10^{21} m³. The high lithium density results in strong lithium line-radiation that dissipates more than 90% of the exhaust power and results in peak wall power loading of ~ 2 MW/m² in the divertor region. The lithium flux from the divertor plate and nearby walls needed to reach these conditions corresponds to evaporation fluxes at surface temperatures in the range of 700-750 C. A key question is the density of lithium ions reaching into the pedestal region a few centimeters inside the magnetic separatrix, which is found to be in the range of 10-20%, implying significant DT fuel dilution in the fusing core. The core lithium level is controlled by the ion and electron thermal force effect along the confining magnetic field lines. The precise value of the ion thermal force is uncertain in these high-density cases, while the electron thermal force values are better understood; removing the ion thermal force effect results in a factor of ~ 2 reduction in the core lithium level. The core lithium level roughly scales as $P_{\text{SOL}}/(n_{\text{core}})^2$, where P_{SOL} is the power flux into the scrape-off layer and n_{core} is the DT density in the edge of the core region. The power scaling can be affected by introducing a moderate-Z impurity such as neon or argon to radiate some of the core power in the edge region, but limited studies with neon show a modest effect; argon should be analyzed in future work. While the base cases assume that DT ions and atoms are fully pumped when they flow to the lithium surfaces, lithium-hydride formation is known to be temperature dependent. But even if the hydride formation is limited (small pumping), the basic properties of the radiative solutions remain largely unchanged. Simulations show only small differences in the lithium solutions for DT pumping in the range of 5-100% and may extend to even smaller pumping rates. The DT particle fluxes to the lithium walls are concentrated in the divertor region, but their magnitude is controlled by the total DT particle flux across the separatrix. Base cases have peak DT wall fluxes of $\sim 2 \times 10^{21}$ particles/(m² s) when the total DT throughput is $\sim 1 \times 10^{23}$ particles/s. This wall flux is quite insensitive to the assumed DT ion/atom pumping rates because such changes primarily affect the DT ion and atom divertor densities rather than the wall-fluxes.

6.3. Liquid Metal Experiments

The Center for Plasma Material Interactions (CPMI) at the University of Illinois specializes in understanding the science behind plasma material interactions and

development of technologies behind plasma facing components. In particular, CPMI has a focus on developing and understanding liquid lithium and other liquid metal technology in the context of how it can be best used in fusion devices. Latest results from CPMI’s toroidal fusion device HIDRA and the latest results on the lithium-metal infused trenches are reported [7]. A full-size LiMIT limiter plate is being built and will be tested in CPMI’s toroidal fusion device HIDRA. Concurrently an all high-Z FLiLi limiter plate fabricated by PPPL will also be tested in HIDRA. The LiMIT and FLiLi are two concepts to flow lithium down the front face; due to HIDRA’s five-fold symmetry, a direct comparison between the two plates can be performed. Different aspects of these technologies will be tested for reliability before or in parallel with full deployment in EAST. A new version of LiMIT is being developed using a mesh of refractory metals to test out new ideas in using TEMHD drive to flow liquid metals. Finally results from the first active lithium hydrogen/deuterium (LiHD) distillation system will be explored. LiHD will eventually be part of a fully integrated liquid lithium loop system being proposed at CPMI to study not only the recycling effects of lithium, but also the absorption rates and the technology needed to retrieve hydrogenic species (e.g. deuterium and tritium which are reactor fuel) and re-use back in the device.

6.4. Flowing Liquid Metal PFC Simulations and Design Exploration

Utilizing an already established fusion design, the Fusion Nuclear Science Facility (FESS-FNSF), free-surface LM flows [8] were explored to establish critical design parameters. The reference design is a tokamak-based machine with 518 MW fusion power, 4.8 m major radius, 1.2 m minor radius and a machine average neutron wall loading $\sim 1 \text{ MW/m}^2$. For this design, a PFC concept that implements a flowing LM first wall and an open-surface divertor is developed. The flowing LM first removes the surface heat flux from the FW and then proceeds to the lower section of the vacuum chamber to form a large LM surface for absorbing high-peak surface heat flux in the divertor region. In pursuing the application of large open LM surfaces in the FNSF, two new computer codes have been developed and then applied to the analysis of free-surface magnetohydrodynamic (MHD) flows and heat transfer, including fast thin flowing liquid layers over the solid FW (“liquid wall”), a “tub-like divertor” and a “fast flow divertor”. The analysis is aimed at optimization of the liquid wall design by matching certain proposed design criteria and also at evaluation of the maximum heat fluxes, using liquid Lithium (Li) as a working fluid. It was demonstrated that the flowing Li FW can tolerate a surface heat flux up to 1 MW/m^2 , while the open-surface Li divertor can remove a maximum peak heat flux of 10 MW/m^2 .

7.0 LM PFC Concepts, and the Research for Liquid Metal Plasma Facing Components

The LM PFC concepts themselves provide a valuable organizing principle for R&D in this area, since many viability aspects are tied to the geometry, environment, and operation characteristics. Recent concepts under consideration include 1) flowing LMs over a surface (first wall or divertor) [8], 2) capillary systems distributed over a surface (first wall or divertor) [113-115], 3) lithium gas/vapor box divertors [44-46], 4) tub-like divertors [8, 116], and 5) LM jets in the divertor [117-120]. These will not be reviewed in this report, but particular aspects will be identified when exploring experimental facilities and capabilities.

A series of parameters can be developed that describe a concept's operation and environment the LM PFC must exist in. Here we are using the FNSF configuration and establishing a LM PFC option in an otherwise conventional fusion device design. These directly inform the experimental apparatus' attributes and upgrade path to more prototypical parameters, that is required to study the LM PFC system. Some of these are listed below,

- B-field magnitude and variations
- LM flow speeds
- LM injection and recovery schemes
- Temperatures
- LM Thickness
- Plasma heat flux
- Plasma particle flux
- LM constituency, base and impurities
- Geometry of flow path
- LM fluid MHD effects
- Substrate materials and their impurities
- Substrate material geometry (e.g. roughening)
- Steady and transient loads (heat, particles)

For example, flowing LM systems are most easily accessed with chute experiments [121,122], where a wide range of LM phenomena can be explored. Clearly the chute (length, width, materials) must be designed to access behavior of interest for the operating parameters. LM MHD behavior can be studied with any liquid metal, such as Galinstan due to its ease of use, while liquid metal specific areas such as corrosion or losses requires the actual liquid metal of interest. Flow geometries (horizontal, vertical, curved, cross-section changes) should be prototyped. Moving toward more prototypical parameters (typical of a fusion device) such as temperatures would ultimately require a vacuum enclosure. Simulating the magnetic field is critical for systems with flow that induce MHD effects, and include all components (toroidal field, normal field, and field gradients) that can impact the flow. It is difficult to achieve the magnetic field strength, anticipated in a fusion device, in one of these experiments, and dimensionless parameters can be used to clarify physics regimes accessible. Although LM safety aspects are always important, safety becomes a critical issue with increasing performance levels in the LM experiment (higher temperature, flow speeds, LM reactivity, high pressure/pumping). Simulation of the plasma exposure, which includes vacuum, heat flux and particle flux, may be difficult to integrate in an offline experiment. Plasma confinement devices (e.g. tokamaks, stellarators) provide useful platforms with self-consistent magnetic fields, particle energy distributions, and geometry, but suffer from low duty cycles and difficulty in diagnosing phenomena of interest. Linear plasma devices are somewhat less self-consistent in their environment (in representing the actual fusion device), but have much higher duty cycle and generally good diagnostic access. Heat (lamps) and plasma particle sources (plasma gun) can be used with offline experiments, to approximate the plasma environment, but might have limited coverage on the LM compared to full extend of the LM flow, for example.

Considering a capillary porous system based on blocks [123], a very similar apparatus can be envisioned for testing, albeit where flow is less critical, although flow induced by overfilling might be of interest as well as recovery of LM if complete evaporation is not practical. The block should have various orientations and a wide range of capillary designs (plasma facing geometry, pore supply geometry, reservoir, substrate materials) would be tested. With the minimization of LM flow aspects, the emphasis shifts to the plasma exposure, capillary fluid dynamics, solid substrate engineering, and large capillary structure versus alignment of many small capillary blocks. With the thin layers typical of capillary concepts the solid substrate strongly participates in power handling.

Recalling the multiple LM properties of interest, and integration needs, these can inform the experiments to be done on the apparatus as well as simulations activities to pursue to develop predictive capability. For example,

- Identifying loss mechanisms from the LM, vacuum interface and plasma
- LM segregation of LM alloys, its sustainment in flowing LM and low flow regimes
- Wetting of LM to substrate materials, full flow regime
- Impurities in the LM, impacts and control
- Hydrogen uptake and removal (hydriding)
- Corrosion of substrate materials by the LM
- Core plasma impact of a LM
- Nuclear properties of LM and modifications to its un-irradiated behavior
- LM properties (solubilities, thermal conductivity, etc.)
- Flow obstructions, first wall penetrations
- Flow over different substrates, conducting and non-conducting
- Impact of B-field gradients and small normal fields on flow
- Injection nozzle optimization
- LM loop and its various apparatus
- Heating, mixing, turbulence

Depending on the LM PFC concept, and the critical behavior to explore, these examinations can require a range of platforms including

- Single to few effect apparatus (e.g. heat flux, hydrogen uptake)
- Plasma/vacuum via confinement device, linear plasma device, or similar
- Loop simulator to explore the hydrogen extraction, LM cleanup, heat exchanger, and corrosion
- Offline flowing/capillary/tub/jet concept experiment (e.g. chute in the case of flowing LM systems)
- Neutron exposure

8.0 Discussion and Conclusions

The use of liquid metals as plasma facing components has potential benefits which can easily be understood to alleviate issues with solid PFCs in the fusion plasma environment. These include the elimination or mitigation of surface heat flux, plasma particle erosion and reconstitution, nuclear damage and transmutation, and strong

gradients in temperature, heating, damage and transmutation. Going beyond these conceptual benefits, it is necessary to explore the practical application of these systems. The liquid metal PFC candidates, Li, SnLi, and Sn have been explored, along with Pb-Li due to its importance for blanket breeding, to identify critical aspects requiring research that can contribute to a strong technical basis for LM PFCs. Of the low melting temperature elements with low evaporation rates over 300-800 °C, Li, Sn-Li, Sn, Ga, Ga-Li, In, In-Li, and Pb-Li were identified. However, Ga and In have resource complications and Ga has aggressive corrosion of steels, and were eliminated.

Liquid metals in the plasma chamber are subject to losses (ultimately entering the plasma) which strongly limit their operating temperature, composed of sputtering, ad-atom, and evaporation. More precise prescriptions are required primarily for the ad-atom component, lower energy range data is required for sputtering, and self-consistent physics treatments of the complex interface of LM-surface, sheath, vapor, and plasma environment.

The tolerable plasma content of the LM candidates can be established that do not compromise the fusion power (or neutron wall load), the divertor heating, and current drive efficiency, and are tied back to the maximum allowed losses from the PFCs.

In the case of LM alloys, such as Sn-Li, the possibility of surface tension induced segregation of Li to the surface may provide some beneficial properties compared to Sn or Li alone. This area requires more research to establish whether it can be created and sustained in a prototypical LM PFC situation.

The wetting of LMs to their solid substrates is absolutely essential to capillary PFC concepts, however their importance to large scale fast flowing LM's is less clear. The behavior of wetting is dependent on the LM and substrate, their impurities, time, and temperature, indicating that prototypical conditions of a LM PFC are needed to properly understand its effects in a fusion device.

Hydrogen uptake and retention is important due to the presence of large quantities of deuterium and tritium in contact with the PFCs in the plasma chamber. Although Sn and Sn-Li appear to behave like solid metal PFCs with low retention, Li has very high uptake and retention. The possibility of hydriding (formation of LiH as a solid in Li solution) is a serious concern for Li and requires further investigation, and is expected to depend on the LM PFC concept, with very thin LM layer and slow moving concepts the most susceptible.

It is important for the LM PFC community to begin characterizing the LM's composition, particularly the impurities in these LM's on a routine basis. Historically LM impurities have been found to impact basic LM properties as well as their interactions with solid substrates. This includes surface contamination in a wide range of experiments with free-surface LMs. In addition, corrosion products from the substrate materials and other materials in the LM loop will also be present in the LM, and all impurities will be exposed to neutrons in the plasma chamber. A significant effort is required to understand and control the constituency of the LM, by identifying impurity sources and establishing the required cleanup technologies.

A unique exploration of the nuclear impacts of LM PFCs shows that since the LMs of interest for the PFC application (Li, Sn, and SnLi) have strong nuclear reactivity they can have benefits on tritium breeding, material damage and He/H production, when the LM layer thickness is > 2 cm. LM PFC concepts that have very thin layers (~ 1 mm) would generally have only weak impacts compared to a case with no LM PFC, and the differences between liquid metals would be minor.

For the LM concepts considered in this study, a solid substrate is required. Due to the proximity of the substrate to the plasma, it must be a fusion relevant structural material, such as reduced activation ferritic martensitic (RAFM) steel or one of its more advanced variants. Corrosion of the substrate by the LM is the major issue, although the substrate does constrain the LM operating temperature. Li demonstrates weak corrosion of steels in flowing tests, although data on corrosion in a magnetic field is missing. Pb-Li has received considerable attention in the corrosion area due to its popularity as the blanket breeder material. For comparison, it reaches thinning of 0.04 mm/yr for static tests, ~ 0.2 mm/yr for flowing tests, and 0.3-0.4 mm/yr for flow in a B-field. This situation will require some form of amelioration. Sn shows strong corrosion thinning of about ~ 3 -15 mm/yr for steels, which is clearly unacceptable, and amelioration is required. Insulation of flow channel walls is generally required for liquid metal flows in order to reduce the pressure drop (drag), and free-surface flows also benefit from this, particularly since many LM PFC concepts have high flow speeds. The data on interaction of LMs with insulator materials is very sparse and must improve considerably. Insulating materials are needed both near the plasma where the LM is a PFC, but also in feed lines and injectors used to bring the LM from outside the fusion core into the plasma chamber.

The effect often referred to as liquid metal embrittlement (LME) is a real showstopper for any liquid metal – solid substrate combination that shows this behavior. The LM penetrates the solid through grain boundaries, cracks or defects and causes rapid embrittlement and crack propagation, when the solid is in tension. Regardless of whether the crack propagation takes milliseconds or months, it is unacceptable in a fusion power system. All LM-solid combinations that exist in the fusion facility under normal or accident conditions must be cleared for this phenomena. Of the LM candidates considered here, only Li has been identified as an LME pair with some specific steels that are not considered fusion relevant. Unfortunately, the understanding of LME is still incomplete and empirical.

Any LM PFC will actually be a LM loop that recirculates the LM, and contains as major components, the plasma chamber, tritium extraction, heat exchanger, cleanup systems and constituency control. Around this loop the LM would have varying temperature, major and impurity constituents, and flow speeds. The sources and sinks for these would be distributed around the loop. Understanding the loop behaviors is critical to establishing the credibility of a LM, for example, the tritium content, or the activated constituent inventories, and the potential for deposition of LM components within the loop.

One potential advantage of LM PFC's is to remove the surface heat flux that would normally be incident on a solid PFC surface. In a fusion power plant this can be about

20% of the available thermal power that is converted to make electricity. Due to temperature limitation of LMs, to avoid excess losses, and the requirement that LM inlet temperatures must not be below 350 °C for the RAFM steel substrates, the design windows for LM PFCs can be quite limited. There are other possible temperature limitations such as corrosion as well. It is not clear that any of the LM candidates can be effectively used in the thermal conversion cycle, even Sn may be severely constrained by its corrosion behavior.

Tritium handling is a major technical aspect of any fusion device, and in the particular case of Li as a LM PFC it takes on a different nature. Since the Li is introduced into the plasma chamber and has contact with the D and T fueling, as well as tritium bred in the Li itself, it can contain a very large tritium inventory, compared to what is typically in a LM breeder loop, for example. Since the burnup of tritium (and deuterium) fuel is expected to be low, a large amount of excess tritium is injected and exhausted from the plasma chamber, ranging from 10-100x the amount that is consumed. With a Li PFC all this tritium is expected to end up in the Li, due to its strong hydrogen uptake, although some may be pumped out with He and other non-condensables. In a device with solid PFCs, or a LM PFC with low hydrogen uptake and retention, this fueling inventory would be in a gaseous loop, exhausted from the plasma chamber with a vacuum pump. Lithium's high solubility for hydrogen can be viewed as an advantage in reducing permeation, however, in an accident scenario the Li could release the tritium in a fire. An examination of this can be found in ref. [4].

Other integration aspects include He pumping which is required to avoid buildup in the plasma core, accommodating penetrations for plasma heating and current drive, pumping LMs into the plasma chamber and getting them back out, and detailed descriptions of the magnetic fields and flow geometries in assessing LM PFCs.

The R&D required to establish a credible database for LM PFCs involves addressing several issues associated with the liquid metals themselves, their interactions with solid substrate materials, integration of LM PFCs into the fusion plant, and the various physics of the individual concepts themselves. Continued activities in design of LM PFCs for a fusion device provides a much-needed focus for R&D toward prototypical parameters and environments. The complexity of liquid metal behaviors requires a simultaneous dedicated simulation development thrust appropriately validated with experiments.

Acknowledgements

This material is based upon work supported by the U.S. DoE, Office of Science, Office of Fusion Energy Sciences, under contracts DE-AC02-76CH03073 (PPPL), DE-AC09-08SR22470 (SRNL), DE-AC52-06NA25396 (LANL), DE-AC52-07NA27344 (LLNL), DE-AC05-00OR22725 (ORNL), DE-AC07-05ID14517 (INL).

References

- [1] C. E. Kessel et al, *Fusion Eng. Des.*, **135**, (2018), 236;
<https://doi.org/10.1016/j.fusengdes.2017.05.081>
- [2] T. D. Rognlien and M. E. Rensink, this conference
- [3] A. Khodak, this conference
- [4] P. W. Humrickhouse, this conference
- [5] T. Bohm, this conference
- [6] J. P. Blanchard, this conference
- [7] D. Andruczyk, this conference
- [8] S. Smolentsev et al, this conference
- [9] M. Abdou et al, *Fusion Eng. Des.*, **54**, (2001), 181.
- [10] R. E. Nygren et al, *Fusion Eng. Des.*, **72**, (2004), 181.
- [11] Y. Hirooka et al, *Fus. Sci. Technol.*, **68**, (2015), 477.
- [12] M. A. Jaworski, A. Khodak, and R. Kaita, *Plasma Phys. Control. Fusion*, **55**, (2013), 124040.
- [13] F. L. Tabares, *Plasma Phys. Control. Fusion*, **58**, (2015), 014014.
- [14] M. Kondo and Y. Nakajima, *Fusion Eng. Des.*, **88**, (2013), 2556.
- [15] J. Yin et al, *J. Alloys Compounds*, **393**, (2005), 105.
- [16] P. Hubberstey et al, *J. Nucl. Mater.*, **191-194**, (1992), 283.
- [17] J. Sangster and A. D. Pelton, *J. Phase Equilibria*, **12**, (1991), 33.
- [18] W. A. Alexander et al, *Can. J. Chem.*, **54**, (1976), 1052.
- [19] J. P. Allain et al, *J. Nucl. Mater.*, **290-293**, (2001), 33.
- [20] J. P. Allain et al, *J. Nucl. Mater.*, **290-293**, (2001), 180.
- [21] M. D. Coventry et al, *J. Nucl. Mater.*, **313-316**, (2003), 636.
- [22] R. P. Doerner et al, *J. Nucl. Mater.*, **290-293**, (2001), 166.
- [23] R. P. Doerner et al, *J. Nucl. Mater.*, **313-316**, (2003), 383.
- [24] R. P. Doerner and S. I Krasheninnikov, *J. Appl. Phys.*, **95**, (2004), 4471.
- [25] R. P. Doerner et al, *J. Nucl. Mater.*, **337-339**, (2005), 877.
- [26] J. P. Allain et al, *J. Nucl. Mater.*, **313-316**, (2003), 641.
- [27] T. D. Rognlien and M. E. Rensink, *Fusion Eng. Des.*, **135**, (2018), 380.
- [28] T. D. Rognlien and M. E. Rensink, *J. Nucl. Mater.*, **290-293**, (2001), 312.
- [29] T. Abrams, et al, *Nucl. Fusion*, **56**, (2016), 016022.
- [30] D. Post et al, *At. Data Nucl. Data Tables*, **20**, (1977), 397.
- [31] W.-H. Shih and D. Stroud, *Phys. Rev. B*, **22**, (1985), 32.
- [32] J. Lee et al, *Materials Trans.*, **45**, (2004), 2864. (Japanese Institute of Metals)
- [33] R. Bastasz and J. A. Whaley, *Fusion Eng. Des.*, **72**, (2004), 111.
- [34] R. Bastasz and W. Eckstein, *J. Nucl. Mater.*, **290-293**, (2001), 19.
- [35] J. P. S. Loureiro et al, *Fusion Eng. Des.*, **117**, (2017), 208.
- [36] B. B. Alchagirov et al, *Russian J. Phys. Chem A*, **90**, (2016), 2262.
- [37] V. Z. Kanchukoev et al, *High Temperature*, **47**, (2009), 292.
- [38] P. F. Adams, et al, *J. Less-Common Metals*, **42**, (1975), 325.
- [39] P. Hubberstey et al, *J. Less-Common Metals*, **49**, (1979), 253.
- [40] E. Veleckis et al, *J. Phys. Chem.*, **78**, (1974), 1933.
- [41] F. J. Smith et al, *J. Inorg. Nucl. Chem.*, **41**, (1979), 1001.
- [42] H. U. Borgstedt and C. Gumiński, *J. Phys. Chem. Ref. Data*, **30**, (2001), 846-865.
- [43] C. E. Messer et al, *J. Phys. Chem.*, **62**, (1958), 220.

- [44] Golubchikov et al, *J. Nucl. Mater.*, **233-237**, (1996), 667.
- [45] Y. Nagayama, *Fusion Eng. Des.*, **84**, (2009), 1380.
- [46] R. J. Goldston et al, *Physica Scripta*, **2016**, (2016), 014017.
- [47] N. Eustathopoulos, *Metals*, **5**, (2015), 350; www.mdpi.com/journal/metals.
- [48] B. Komolafe and M. Medraj, *J. Metallurgy*, **2014**, article ID 387046; <http://dx.doi.org/10.1155/2014/387046>.
- [49] H. Nakae et al, *Materials Trans.*, **33**, (1992), 400. (Japanese Institute of Metals)
- [50] J. Luo, *Corrosion*, **72**, (2016), 897.
- [51] P. Fiflis et al, *Fusion Eng. Des.*, **89**, (2014), 2827.
- [52] S. Smolentsev, *Theor. Comput. Fluid Dyn.*, **23**, (2009), 557.
- [53] C. Choi and M. Kim, *Wettability Effects on Heat Transfer, Two Phase Flow, Phase Change and Numerical Modeling*, (2011), ISBN:978-953-307-584-6; <http://www.intechopen.com/books/two-phase-flow-phase-change-and-numerical-modeling/wettability-effects-on-heat-transfer>.
- [54] M. Hvasta, “Designing and Optimizing a Moving Magnet Pump for Sodium Systems”, <http://adsabs.harvard.edu/abs/2013PhDT.....155H>.
- [55] M. J. Baldwin et al, *Nucl. Fusion*, **42**, (2002), 305.
- [56] J. M. Canik et al, *Phys. Plasma*, **18**, (2011), 056118.
- [57] D. P. Boyle et al, *Plas. Phys. Control. Fusion*, **53**, (2011), 105011.
- [58] J. S. Hu et al, *Fusion Eng Des*, **89**, (2014), 2875.
- [59] T. H. Osbourne et al, *Nucl. Fusion*, **55**, (2015), 063018.
- [60] E. Wolfrum et al, *Nucl. Mater. Energy*, **12**, (2017), 18.
- [61] P. S. Krstic et al, *Phys. Rev. Lett.*, **110**, (2013), 105001.
- [62] E. Oyarzabal et al, *Fusion Eng Des*, **117**, (2017), 217.
- [63] A. B. Martin-Rojo et al, *Fusion Eng Des*, **89**, (2014), 2915.
- [64] J. P. Tonks et al, *J. Nucl. Mater.*, **484**, (2017), 228.
- [65] P. F. Tortorelli et al, Effects of Nitrogen and Nitrogen Getters in Lithium on the Corrosion of Type 316 Stainless Steel, March 1979, https://inis.iaea.org/collection/NCLCollectionStore/_Public/10/472/10472566.pdf.
- [66] H. Kondo et al, *Nucl. Fusion*, **51**, (2011), 123008.
- [67] K. Natesan et al, *J. Nucl. Mater.*, **307**, (2002), 743.
- [68] J. Neuhausen et al, Mercury Purification in the MW Liquid Metal Spallation Target of EURISOL-DS, http://www.hep.princeton.edu/mumu/target/Neuhausen/neuhausen_accapp07.pdf
- [69] A. Davis et al, *Fusion Eng. Des.*, **135** Part B, (2018), 271.
- [70] M. A. Futterer et al, *J. Nucl. Mater.*, **283-287**, (2000), 1375.
- [71] Liquid Metal Handbook, Ed. R. N. Lyon, 1950.
- [72] M. Kondo et al, *Fusion Engr. Des.*, **98-99**, (2015), 2003.
- [73] M. Kondo et al, *Fusion Engr. Des.*, **136** Part B, (2018), 1581.
- [74] E. E. Hoffman and R. W. Harrison, “The Compatibility of Refractory Metals with Liquid Metals”, Ed. I. Machlin, in *Refractory Metal Alloys Metallurgy and Technology*, American Institute of Mining, Metallurgical and Petroleum Engineers, 1968.
- [75] J. R. DiStefano and E. E. Hoffman, “Corrosion Mechanisms in Refractory Metal – Alkali Metal Systems”, Oak Ridge National Laboratory report ORNL-3424, 1963: <https://www.osti.gov/scitech/servlets/purl/4635104>
- [76] P. F. Tortorelli and J. M. DeVan, *J. Nucl. Mater.*, **85 & 86**, (1979), 289.
- [77] P. F. Tortorelli and O. K. Chopra, *J. Nucl. Mater.*, **103 & 104**, (1981), 621.

- [78] O. K. Chopra and P. F. Tortorelli, *J. Nucl. Mater.*, **122 & 123**, (1984), 1201.
- [79] O. K. Chopra and D. L. Smith, *J. Nucl. Mater.*, **133 & 134**, (1985), 861.
- [80] K. Shibata et al, *J. Nucl. Mater.*, **122 & 123**, (1984), 1252.
- [81] O. K. Chopra and D. L. Smith, *J. Nucl. Mater.*, **141-143**, (1986), 584.
- [82] M. Kondo et al, “Flow Accelerated Corrosion and Erosion-Corrosion of RAFM Steel in Liquid Breeders”, NIFS-993, National Institute for Fusion Studies, Japan, 2012; <http://www.nifs.ac.jp/report/NIFS-993.pdf>
- [83] J. H. DeVan, J. E. Selle, and A. E. Morris, “Review of Lithium Iron-Base Alloy Corrosion Studies”, ORNL/TM-4927, Oak Ridge National Laboratory, 1976; <https://www.osti.gov/servlets/purl/4087807>
- [84] B. A. Pint et al, *Mater. High Temp.*, **29**, (2012), 129.
- [85] A. S. Sree et al, “Preliminary corrosion studies of IN-RAFM steel with stagnant Lead Lithium at 550 C”, 2017, <https://arxiv.org/pdf/1706.05000.pdf>
- [86] M. Kondo et al, *Fusion Eng. Des.*, **125**, (2017), 316.
- [87] J. Konys et al, *J. Nucl. Mater.*, **417**, (2011), 1191.
- [88] J. Konys et al, *J. Nucl. Mater.*, **455**, (2014), 491.
- [89] W. Krauss et al, *Nucl. Mater. And Energy*, **9**, (2016), 512.
- [90] E. Plantacis et al, “Corrosion Phenomena of Eurofer Steel in Pb-17Li Stationary Flow at Magnetic Field”, Int'l Conference on Nuclear Engineering (ICON14), July 2006, Florida, USA;
- [91] A. S. Sree et al, *Nucl. Fusion*, **54**, (2014), 083029.
- [92] M. C. Gazquez et al, *J. Nucl. Mater.*, **465**, (2015), 633.
- [93] M. Kondo et al, *Fusion Eng. Des.*, **98-99**, (2015), 2003.
- [94] A. Heinzel et al, *Materials and Corrosion*, **68**, (2017), 831.
- [95] A. R. Petrova et al, “The Selection of Materials Resistant to Molten Tin at High Temperature”, *Metal Science and Heat Treatment*, 11, (1969), 819; <https://doi.org/10.1007/BF00652062>
- [96] B. A. Pint et al, *JOM*, **68**, (2014), 2458.
- [97] S. Majumdar et al, *J. Nucl. Mater.*, **486**, (2017), 60.
- [98] F. Barbier and J. Blanc, *J. Mater. Res.*, **14**, (1999), 737.
- [99] H. Kamdar, “Embrittlement by Liquid Metals”, UCLA-ENG-7234, April 1972, *Treatise on Materials Science and Technology*, **25**, (1983), 361.
- [100] W. Rostoker, J. M. McCaughey, and H. Markus, “Embrittlement by Liquid Metals”, Reinhold Publishing Corporation, New York, 1960.
- [101] M. G. Nicholas and C. F. Old, *J. Mater. Science*, **14**, (1979), 1.
- [102] S. G. Keller and A. P. Gordon, *Eng. Fracture Mechanics*, **84**, (2012), 146.
- [103] J. C. Hirvonen et al, “Use of Liquid Metal Embrittlement for Controlled Fracture”, Army Research Laboratory, ARL-TR-4976, September 2009.
- [104] J. Zhang et al, *J. Nucl. Mater.*, **404**, (2010), 82.
- [105] R. Viswanathsan et al, “Materials Technology for Advanced Coal Power Plants”, <https://www.phase-trans.msm.cam.ac.uk/2005/LINK/188.pdf>.
- [106] M. S. Tillack et al, *Fusion Sci. Technol.*, **67**, (2015), 49.
- [107] X. Wang et al, *Fusion Sci. Technol.*, **67**, (2015), 193.
- [108] A. Hassanein, *J. Nucl. Mater.*, **302**, (2002), 41.
- [109] M. Nieto et al, *J. Nucl. Mater.*, **313-316**, (2003), 646.
- [110] C. E. Kessel et al, *Fusion Eng. Des.*, **135** Part B, (2018), 356.
- [111] H. Katsuda et al, *Fusion Sci. Technol.*, **30**, (1996), 1152.
- [112] P. Humrickhouse et al, *Fusion Eng. Des.*, **135** Part B, (2018), 302.

- [113] V. A. Evtikhin et al, *Fusion Eng. Des.*, **49-50**, (2000), 195.
- [114] S. V. Mirnov et al, *Fusion Eng. Des.*, **65**, (2003), 455.
- [115] M. A. Jaworski et al, *Plas. Phys. Control. Fusion*, **55**, (2013), 124040.
- [116] M. Shimada and Y. Hirooka, *Nucl. Fusion*, **54**, (2014), 122002.
- [117] N. B. Morley et al, *Fusion Sci. Technol.*, **34**, (1998), 1035.
- [118] S. V. Mirnov et al, *J. Nucl. Mater.*, **196-198**, (1992), 45.
- [119] R. Moir, “Jets and droplets compared to a moving slab of liquid for divertor cooling for a tokamak magnetic fusion energy reactor”, 2012,
http://www.ralphmoir.com/wp-content/uploads/2012/10/jetdrop_031708.pdf
- [120] J. Miyazawa et al, *Fusion Eng. Des.*, **125**, (2017), 227.
- [121] A. Ying et al, *Fusion Eng. Des.*, **72**, (2004), 35.
- [122] M. D. Nornberg et al, *Rev. Sci. Instru.*, **79**, (2008), 094501.
- [123] P. Rindt et al, *Fusion Eng. Des.*, **112**, (2016), 204.